APPLICATION OF SUPERPARAMAGNETIC MESOPOROUS SILICATES ON
NAPROXEN REMOVAL

Miss Waritta Ruangtrakul

A Thesis Submitted in Partial Fulfillment of the Requirements
for the Degree of Master of Science Program in Environmental Management
(Interdisciplinary Program)
Graduate School
Chulalongkorn University
Academic Year 2010

การประยุกต์ใช้เมโซพอรัสซิลิเกตที่มีคุณสมบัติซูเปอร์พาราแมกเนติกในการกำจัดนาพรอกเซน

นางสาว วริษฐา เรืองตระกูล

วิทยานิพนธ์นี้เป็นส่วนหนึ่งของการศึกษาตามหลักสูตรปริญญาวิทยาศาสตรมหาบัณฑิต

สาขาวิชา การจัดการสิ่งแวดล้อม (สหสาขาวิชา)

บัณฑิตวิทยาลัย จุฬาลงกรณ์มหาวิทยาลัย

ปีการศึกษา 2553

Thesis Title	APPLICATION OF SUPERPARAMAGNETIC MESOPOROUS SILICATES ON NAPROXEN REMOVAL
By	Miss Waritta Ruangtrakul
Field of Study	Environmental Management
Thesis Advisor	Assistant Professor Patiparn Punyapalakul, Ph.D.

_____

Accepted by the Graduate School, Chulalongkorn University in Partial Fulfillment of the Requirements for the Master's Degree

………………………………… Dean of the Graduate School

(Associate Professor Pornpote Piumsomboon,Ph.D.)

THESIS COMMITTEE

………………………………… Chairman

(Assistant Professor Chantra Tongcumpou, Ph.D.)

………………………………… Thesis Advisor

(Assistant Professor Patiparn Punyapalakul, Ph.D.)

………………………………… Examiner

(Associate Professor Jin Anotai, Ph.D.)

………………………………… Examiner

(Assistant Professor Chawalit Ngamcharussivichai, Ph.D.)

………………………………… External Examiner

(Punjaporn Weschayanwiwat, Ph.D.)

วริษฐา เรืองตระกูล : การประยุกต์ใช้เมโซพอรัสซิลิเกตที่มีคุณสมบัติซูเปอร์พาราแมกเนติกใน การกำจัดนาพรอกเซน (APPLICATION OF SUPERPARAMAGNETIC MESOPOROUS SILICATES ON NAPROXEN REMOVAL) อ. ที่ปรึกษาวิทยานิพนธ์หลัก: ผศ.ดร.ปฏิภาณ ปัญญาพลกุล, 103 หน้า.

งานวิจัยนี้ได้ศึกษาประสิทธิภาพการดูดซับยาชนิดนาพรอกเซนโดยมีโซพอรัสซิลิเกตที่มี คุณสมบัติซูเปอร์พาราแมกเนติกในน้ำเสียสังเคราะห์ที่ความเข้มข้น 0.5 ถึง 10 มิลลิกรัมต่อลิตร ตัวกลาง ดูดซับทั้งหมดสามารถสังเคราะห์ได้โดยการใช้สารลดแรงตึงผิวเป็นแม่แบบ (Surfactant Template)และ ปรับปรุงพื้นที่ด้วยการต่อติดหมู่ฟังก์ชันที่แตกต่างกัน 3 ชนิดโดยวิธีโค-คอนเดนเซชั่น (Co-condensation) ได้แก่ หมู่ ซิลานอล หมู่อะมิโน หมู่เมอแคปโต หมู่ไนไตร และ หมู่ฟีนอล อัตราเร็วการ ดูดซับนาพรอกเซนสอดคล้องกับสมการปฏิกิริยาอันดับสองเสมือน ไอโซเทอมการดูดซับนาพรอกเซน สอดคล้องกับสมการทั้งแบบเส้นตรง ฟรุนด์ลิชและ แลงเมียร์ จากผลการทดลองพบว่ามีโซพอรัสซิลิ เกตที่คุณสมบัติซูเปอร์พาราแมกเนติกที่ต่อติดหมู่ฟังก์ชันฟีนอลมีประสิทธิภาพการดูดซับสูงสุด ตาม ด้วยหมู่เมอแคปโต หมู่ไนไตร หมู่ซิลานอล และ หมู่อะมิโนตามลำดับ แต่ยังคงมีประสิทธิภาพน้อยกว่า ถ่านกัมมันต์ชนิดผง ตัวกลางดูดซับที่ไม่ชอบน้ำมีประสิทธิภาพการดูดซับนาพรอกเซนได้สูงกว่า ตัวกลางดูดซับที่ชอบน้ำ ส่วนแรงระหว่างประจุมีผลต่อการดูดซับนาพรอกเซนทุกหมู่ฟังก์ชันบนพื้นผิว ยกเว้นหมู่ อะมิโนและหมู่ซิลานอล

ตัวกลางดูดซับสามารถแยกออกจากน้ำโดยใช้แรงแม่เหล็กเหนี่ยวนำตัวกรอง (High Gradient Magnetic Separation filter) ผลการทดลองพบว่าความยาวตัวกรอง อัตราเร็วของน้ำ พื้นที่ผิวตัวกรอง และ ความเข้มข้นของตัวกลางดูดซับมีผลต่อเส้นเบรคทรู (Breakthrough curve) การเพิ่มความยาวตัว กรอง การลดอัตราเร็วของน้ำ และการลดความเข้มข้นตัวกลางดูดซับจะทำให้เพิ่มเวลาในการเบรคทรู (Breakthrough Time) นอกจากนั้นการกรองโดยใช้แม่เหล็กเหนี่ยวนำตัวกรองสามารถประยุกต์ใช้ได้กับ สมการบีดีเอสที (BDST model)เนื่องจากมีค่าสัมประสิทธิ์ของการตัดสินใจ (R^2)สูง อย่างไรก็ตาม สมการบีดีเอสที (BDST model) ไม่สามารถใช้ได้เมื่ออัตราเร็วของน้ำและความเข้มข้นของตัวกลางดูด ซับเปลี่ยนแปลง

สาขาวิชาการจัดการสิ่งแวดล้อม   ลายมือชื่อนิสิต ....

ปีการศึกษา 2553   ลายมือชื่ออ.ที่ปรึกษาวิทยานิพนธ์หลัก...

5287566920: MAJOR   ENVIRONMENTAL MANAGEMENT

KEYWORDS: SUPERPARAMAGNETIC HEXAGONAL MESOPOROUS SILICATES / NAPROXEN / ADSORPTION / HIGH GRADIENT MAGNETIC SEPARATION FILTER

WARITTA RUANGTRAKUL : APPLICATION OF SUPERPARAMAGNETIC MESOPOROUS SILICATES ON NAPROXEN REMOVAL. ADVISOR: ASSIST. PROF. PATIPARN PUNYAPALAKUL, Ph.D., 103 pp.

Adsorption of Naproxen (NAX), non-steroidal anti-inflammatory drug (NSAID), by using superparamagnetic hexagonal mesoporous silicates (HMS-SP) in synthetic wastewater at high concentration (0.5 – 10 mg/L) was investigated. Five different types of adsorbents were synthesized by surfactant templating method, and modified surface functional group with silanol, 3-aminopropyltriethoxy-, 3-mercaptopropyl-, phenyltrimethoxy- and butyronitrile- groups by co-condensation method that denoted as HMS-SP, A-HMS-SP, M-HMS-SP, P-HMS-SP and N-HMS-SP, respectively. Kinetic adsorptions of all synthesized adsorbents were fitted well with pseudo-second-order equation. Adsorption isotherms were best matched with linear model, Fruendlich model and Langmuir model. P-HMS-SP had highest adsorption capacity following with M-HMS-SP, N-HMS-SP, HMS-SP and A-HMS-SP, but still lower than PAC. Hydrophobic adsorbents had higher adsorption capacity of NAX than hydrophilic adsorbents. Electrostatic interaction can affect NAX adsorption capacities of adsorbents, except for A-HMS-SP and HMS-SP.

High Gradient Magnetic Separation filter (HGMS filter) was applied to separate adsorbent particle from treated water. Effect of bed depth, flow rate, surface area of stainless filer and concentration of particle influenced on the breakthrough curve. The breakthrough time was increasing by extending bed depth of stainless filter and decreasing flow rate and particle concentration. Moreover, application of BDST model can be matched with HGMS filter, due to high correlation coefficient. Nevertheless, BDST model cannot apply with changing flow rate and particle concentration.

Field of Study: Environmental Management   Student's Signature ……………………………

Academic Year: 2010   Advisor's Signature ……………………………

ACKNOWLEDGEMENTS

CONTENTS

LIST OF TABLES

Table   **Page**

LIST OF FIGURES

Figure   **Pages**

LIST OF ABBREVIATIONS

A-HMS-SP	=	3-aminopropyltrimethoxy surface functional group grafted on superparamagnetic mesoporous silicates
CAS	=	Conventional Activated sludge
F-HMS-SP	=	Functionalized hexagonal mesoporous silicate
HGMS	=	High gradient magnetic separation
HMS	=	Hexagonal mesoporous silicate
HMS-SP	=	Superparamagnetic hexagonal mesoporous silicate
M-HMS-SP	=	3-mercaptopropyltrimethoxy surface functional group grafted on superpapramagnetic mesoporous silicate
NAX	=	Naproxen
N-HMS-SP	=	4-triethoxysilyl butyronitrile surface functional group grafted on superpapramagnetic mesoporous silicate
NSAID	=	Non-Steroidal Anti-Inflammatory Drug
PAC	=	Powder activated carbon
P-HMS-SP	=	Phenyltrimethoxy functional group grafted on superpapramagnetic mesoporous silicate
SP-MS	=	Superparamagnetic mesoporous silicate
T	=	Tesla
Breakthrough time	=	The time that reach to the minimum concentration in the effluent

LIST OF NOMENCLATURES

d_m	=	Media diameter (m)
d_p	=	Diameter of adsorbent particle (m)
v_0	=	Velocity rate (m/s).
ω	=	The angular velocity (rad/s)
ε	=	Porosity of media filter.
η_{Diff}	=	Diffusion efficiency
η_{int}	=	Interception efficiency
η_{sed}	=	Sedimentation efficiency
μ_0	=	Magnetic permeability of vacuum (Wb/(A·m)),
μ_c	=	Viscosity of solution (kg/(m·s))
μ_m	=	Magnetic permeability of material (Wb/(A·m))
ρ_p	=	Density of particle (kg/m^3),
ρ_g	=	Density of fluid (kg/m^3)
$\Delta\rho$	=	Difference of media and adsorbent particle density (g/cm^3)
∇H	=	The gradient of magnetic strength field at the position of the particle.
1/n	=	Freundlish intensity parameter.
A_0	=	Cross section area (m^2)
B	=	Magnetic flux density (T or Wb/m^2)
C	=	Concentration (mg/L)
C	=	The thickness boundary layer(m).
F_c	=	Centrifugal force (N),
F_d	=	Drag force (N)
F_g	=	Gravitational force (N),
F_m	=	Magnetic force (N)
g	=	Gravity accelerate (m/s^2).

LIST OF NOMENCLATURES (Continued)

H	=	Magnetic strength field (A/M)
H	=	Depth of media filter (m)
K	=	Boltzmann's constant (1.38×10^{-23} kg·m^2/K·s^2),
k_1	=	Pseudo first rate constant (1/h).
k_2	=	Pseudo second rate constant (g /mg·h).
K_F	=	Freundlish constant related to the adsorption capacity and adsorption intensity of the sorbent
k_{id}	=	The intraparticle rate constant(mg/g·min$^{1/2}$)
K_L	=	Langmuir constant related to the affinity of the binding sites and energy of adsorption (L /mg)
M_p	=	The particle magnetization (A/m)
q_e	=	Adsorption capacity at equilibrium per unit weight of adsorbent (mg/ g),
q_m	=	Adsorption capacity in complete layer (mg/g)
q_t	=	Adsorption capacity at any time (mg/g)
r	=	The radial of the particle (m).
t	=	Time (min.)
T	=	Absolute temperature (K)

CHAPTER I
INTRODUCTION

1.1 State of Problems

The emerging micropollutants such as pharmaceutical residue in natural water are concerned as one of the major issues in the past decade. There are many studies reported that conventional wastewater treatment systems cannot eliminate these persistent substances effectively (Sim et al.,2010). Although, detected concentration of pharmaceutical residue from environment is quite low in µg/L or ng/L level but some substances still has ecotoxicity and can be accumulated in environment.

Naproxen (NAX), non-steroidal anti-inflammatory drug (NSAID), might cause acute and chronic toxic at mg/L level. NAX can be detected in high concentration at 324 mg/L (Mascolo, Balest et al.,2010) from pharmaceutical wastewater stream. Moreover, previous literature reviews reported that phototransformation products of NAX are higher toxic than NAX. Conventional activated sludge (CAS) is commonly used to eliminate NAX , but the efficiency of this method is wide rage (0%-80%) (Nakada et al.,2006). Many researchers found that the physical treatment process could not remove NAX from wastewater effectively. Advance oxidation processes were supposed to have higher removal efficiency of NAX (such as Cl_2 process), however, degradation by-products and their toxicity still have not been investigated yet (Isidori, Lavorgna et al.,2005).

Adsorption is the process used to separate target pollutant from wastewater. Powder activated carbon (PAC) is widely adsorbent that apply to pollutants removal due to their high adsorption capacity. Nevertheless, the weak point of PAC is its low selectivity.

Mesoporous silicates are the materials that have large surface area and uniform pore size. It can be enhanced selective adsorption capacities of target compounds by various methods such as functionalization of organosilane and metal substitution. Moreover, separation efficiency of used adsorbent from wastewater stream can be improved by increasing superparamagnetic characteristics of the adsorbent. The silicate porous materials are widely used to adsorb pollutant particle because their high pore size distribution and high surface area. Moreover, it can be modified surface by organo silane functional group to improve adsorption capacity and selectivity of silicate porous materials. These materials are classified in three class base on pore size: macroporous > 50nm, mesoporous between 2nm and 50nm and microporous < 2nm. Hexagonal mesoporous silicates (HMS) are mostly used due to suitable pore size range.

The superparamagnetic particles are the ferromagnetic materials including iron are smaller than 20-30 nm and contained in single magnetic domain. The particles have small positive susceptibility when applied external field and no net magnetization after removing external field. The magnetite particle (Fe_3O_4) is mostly wide superparamagnetic particle which made from Iron (II) and Iron (III). The particles are coated by silicate porous material that denoted as MS-SP.

To use magnetite as core of adsorbents is improved separation efficiency. It can be separate by apply magnetic properties. The superparamagnetic mesoporous silicates are not only enhance adsorption capacity by grating functional group, but also separation efficiency.

High Gradient Magnetic Separation filter (HGMS filter) is commonly used in magnetic filtration to separate magnetic materials from non-magnetic solution. The mechanism of magnetic filtration is to handle the magnetic particles in magnetic filter media such as stainless steel which induced by the magnetic field. To induce magnetic field by permanent magnet is simply method but might lower the efficiency than by electromagnet or superconducting magnet which are more complicated. The objectives of this study are to investigate adsorption capacities of naproxen (NAX) on functionalized

superparamagnetic mesoporous silicates (SP-MS) comparing with powdered activated carbon (PAC) and to evaluate possibility to separate functionalized SP-MSs by high gradient magnetic separation filter (HGMS filter).

1.2 Objectives

The main objectives of this study are to investigate adsorption capacities of naproxen (NAX) on functionalized superparamagnetic mesoporous silicates (SP-MS) comparing with powdered activated carbon (PAC) and to evaluate possibility to separate functionalized SP-MSs by high gradient magnetic separation filter (HGMS filter). The specific objectives can be expressed as following:

1. To study effects of surface functional groups on adsorption capacity of NAX at high concentration in aqueous phase.
2. To study effects of electrostatic interaction on adsorption of NAX by varying pH.
3. To investigate effects of flow input, depth and surface area of stainless filter on separation efficiency and breakthrough of HGMS filter.
4. To examine effects of particle concentration and adsorbed NAX on the separation efficiency and breakthrough of HGMS filter.

1.3 Hypotheses

1. Each surface functional group might perform different effect on NAX adsorption capacity due to different interactions between surface functional group of adsorbents such as hydrogen bonding, electrostatic force and hydrophobic interaction.
2. The electrostatic force might affect NAX adsorption capacity of synthesized adsorbents.
3. The retention time, particle concentration and surface area of stainless filter might affect efficiency and breakthrough of HGMS filter due to interaction active site.

4. Adsorbed NAX on adsorbent's surface might affect efficiency and breakthrough of HGMS filter due to changing of surface interaction.

1.4 Scopes of the Study

This research was studied at Department of Environmental Engineering, Faculty of Engineering and NCE-EHWM laboratory, Chulalongkorn University. There are four parts of this study which consist of:

1.4.1 Synthesis of Adsorbents

Magnetite (Fe_3O_4), superparamagnetic hexagonal mesoporous silicates (HMS-SP) and functionalized superparamagnetic hexagonal mesoporous silicates (F-HMS-SP) with organic functional groups such as 3-aminopropyltrimethoxy-, 3-mercaptopropyltrimethoxy-, phenyltrimethoxy- and 4-triethoxysilyl butyronitrile functional group.

1.4.2 Characterization of Synthetic adsorbents

Physico-chemical characteristics of synthesized adsorbents were analyzed by various methods such as X-ray diffraction, nitrogen adsorption isotherm, FT-IR spectra, surface charge by zeta potential measurement, elemental analysis and scanning electromicroscopy (SEM).

1.4.3 Adsorption Study of Naproxen (NAX) on Adsorbents

Investigation of adsorption mechanisms of NAX on all adsorbents are divided into 2 parts; adsorption kinetic and adsorption isotherm. Adsorption experiments were conducted under controlled pH temperature and ionic strength. Moreover, effect of pH on NAX adsorption was studied by comparison of isotherms at pH 5, 7 and 9. In this study, NAX concentration was conducted at range of 0.5-10 mg/L. The adsorption results of synthesized adsorbents were compared with powder activated carbon (PAC).

1.4.4   Separation of Adsorbents

The aim of this part is to investigate effects of flow input, depth and surface area of stainless filter and to examine effects of particle concentration and adsorbed NAX on the separation efficiency and breakthrough of HGMS filter.

CHAPTER II

THEORETICAL BACKGROUNDS AND LITERATURE REVIEWS

2.1 Residue of Pharmaceutical

The residue of pharmaceutical products is one of emerging substances in environment because of their consumption volume, toxicity and persistence in the environment.(Fent, Weston and Caminada ,2006; Moldovan ,2006; Mompelat, Le Bot and Thomas ,2009) At present, pharmaceutical products were used widely for human health and veterinary, for example paracetamol (Mompelat et al. ,2009), caffeine, ciprofloxacin and acetaminophen (Sim, Lee and Oh ,2010), etc, and those can be released to environment. Pharmaceutical residue can be detected in very widespread not only in pharmaceutical industrial and hospital wastewater treatment plant but also in domestic treatment plant and surface water. Figure 2.1 shows fate of pharmaceutical residue related to their persistence and bioaccumulation. Moreover, it is not so easy to determine and investigate the quantity of pharmaceutical residue and their effect to environment. **Jones el al.** (2002) demonstrates that pharmaceutical contaminated water is effect to aquatic animal (Fent et al. ,2006; Joon-Woo Kim ,2009). However, ecotoxicological effects of pharmaceuticals on aquatic and terrestrial organisms and wildlife are still unclear. Biological treatment process is mainly process that can efficiently eliminate some of pharmaceutical residues for instance acetaminophen, caffeine and acetylsalicylic acid (Sim et al. ,2010). But, in some case, more advance treatment process is required to remove high persistent pharmaceutical residues such as Diclofenac, Naproxen and Carbamazepine (Klavarioti, Mantzavinos and Kassinos ,2009).
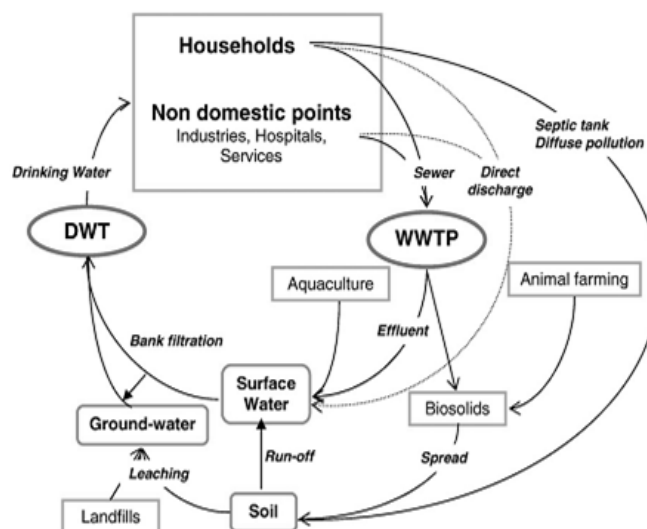
Figure 2.1 Fate of drug transfer (Mompelat et al. ,2009).

2.2 Naproxen (NAX)

Naproxen (NAX) is used to relieve pain, fever, inflammation and stiffness caused by some conditions such as osteoarthritis, kidney stones, rheumatoid arthritis, psoriatic arthritis and gout. It is a NSAID (non-steroidal anti-inflammatory drug) which is a type of pharmaceutical products. NSAIDs have been dominated pharmaceutical residue released to environment and have been detected at high concentration due to it can be used without prescription. NAX is acidic pharmaceutical and most frequently detected substance of NSAIDs. Quantity use of NAX is showed in table 2.1. Table 2.2 demonstrates properties of NAX and Figure 2.2 shows the molecular structure of NAX.
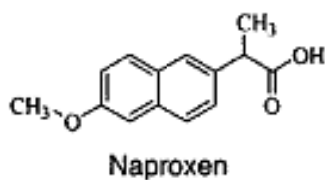
Figure 2.2 Structure of Naproxen.

Table 2.1 Quantity use of Naproxen

Amount Used (tons/year)	Country	Year
35.067[a]	England	2000
22.85[b]	Australian	2004
22-33[c]	Japan	2002
26[d]	Canada	2001
41.133[e]	Korea	2006

[a] Jones et al.,(2002), [b] Khan and Ongerth,(2004), [c] Nakada et al.,(2006), [d] DellaGreca et al.,(2003),and [e] Sim et al.,(2010)

Table 2.2 Physico-chemical Properties of the NAX

Parameters	Descriptions
Molecular weight	230.26[a]
CAS-number	22204-53-1[a]
Molecular diameter	$11.873\dot{A}$
Melting points	153°C
Log K_{ow}	3.18-3.24[b]
Solubility in water	15.9 mg/ l at 25˚C[c]
pKa	4.15[b]
Formula	$C_{14}H_{14}O_3$[d]

[a]Lindqvist, Tuhkanen and Kronberg,(2005), [b]Tixier et al., (2003), [c]Yu, (2008) and [d](Carballa et al. ,2004)

2.3 Ecotoxicity of Naproxen

About ecotoxicity of naproxen, there were a few literatures to investigate. Nevertheless, acute effect of naproxen was studied for each organism which demonstrated in (Fent, Weston et al.,2006),(Cleuvers,2004), and (Isidori, Lavorgna et al.,2005). Researchers reported that acute effect of duck weed, rotifers, and fish are 24.2

mg/L, 62.48 mg/L and 800 to 900 mg/L. Furthermore, the concentration that occur acute effect was in range mg/L. So this unit was not found in environmental concentration. While detected concentration of naproxen in environment was in order of µg/L, there was little to know about long term effects for microorganism and animal. At present, Isidori el at (Isidori et al.,2005) revealed that chronic toxicity values on algae, rotifers and crustaceans were 31.82 mg/L ,0.56 mg/L ,and 0.33 mg/L, and minimum value was 0.11 mg/L on crustaceans. These values shows that naproxen at low concentration might affect environment and ecosystem. The photodegradation of naproxen was occurred in both river and distilled water (Khetan,and Collins,2007). Figure 2.3 showed phototransformation products of naproxen. The products are high toxic than its original form, though it did not influence genotoxicity and mutagenesis. The literatures demonstrated that toxicity of substances depends on hydrophobicity, higher hydrophobicity substances is higher toxic.
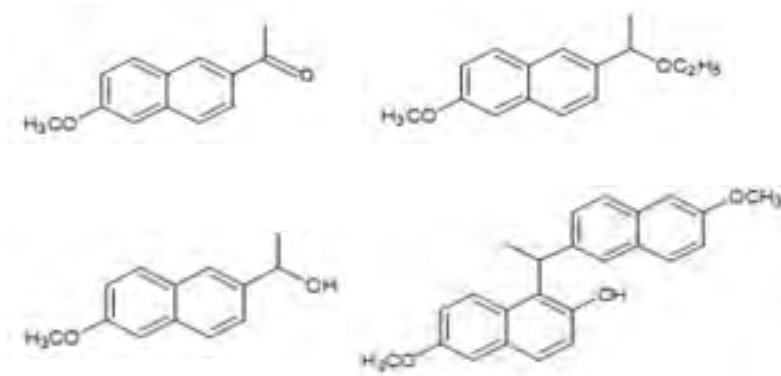
Figure 2.3 Photoproduct of Naproxen(Isidori, Lavorgna et al.,2005).

2.4 Detected Concentration of Naproxen in Environment

For the residue of pharmaceutical product in nature water, naproxen was found in top ten. Table 2.3 shows detected concentration of naproxen.

Table 2.3 Detected Concentration of Naproxen

Country	Source	Concentration	Ref.
Brazil	Surface water	0.020-0.120 µg/L	(Stumpf et al.,1999)
Korea	Surface water Hospital WWTP	0.011-0.013 µg/L 0.077µg/L 0.067-0.195 µg/L	(Sim et al.,2010)
Canada	WWTP	0.36-2.54 µg/L	(Lee et al.,2005)
Greece	WWTP Hospital	ND-0.7 µg/L ND-10.0 µg/L	(Kosma et al.,2010)
USA Canada, USA	WWTP Surface water	81–106 ng/L 22–107 ng/L	(Boyd et al.,2004)
Finland	WWTP	0.16-1.92 µg/L	(Lindqvist et al.,2005)
Spain	WWTP	0.22-4.28 µg/L	(Santos et al.,2007)
Italy	Industrial pharmaceutical wastewater	324 mg/L	(Mascolo et al.,2010)

2.5 Removal of Naproxen

2.5.1 Wastewater Treatment Plant

Wastewater treatment plants consisted of two parts: physicochemical treatment process and biological treatment process. For physicochemical treatment process, it was not effectively in removing pharmaceutical substances, but most pharmaceutical substances were eliminated by biological treatment process (Sim et al.,2010). For removal of naproxen, this process was in wide range, it depend on variation in the functioning of the process for example; Membrane bioreactor (MBR), Conventional activated sludge (CAS), and wetland (Lindqvist ,Tuhkanen and Kronberg ,2005). The literatures revealed that efficient removal of wetland was less than CAS (Matamoros, García et al.,2008),and MBR was high effective than CAS (Kimura, Hara et al.,2005),(Joss, Keller et al.,2005). Nevertheless, not only type of process but also designed parameters such as age of the activated sludge and hydraulic retention time also

affected efficient of NAX removal. However, cause of low degradability of NAX was high hydrophobicity of naproxen. Table 2.4 demonstrated biodegradation of naproxen by conventional activated sludge.

Table 2.4 Biodegradation of Naproxen of Conventional Activated Sludge.

Country	Biodegradation (%)	Ref.
Korea	40-100	(Sim et al.,2010)
Japan	0-80	(Nakada et al.,2006)
Swiss	65-80	(Joss et al.,2005)
Japan	27-79	(Kimura et al.,2007)
USA	6.3	(Reclamation,2009)

2.5.2   Advance Oxidation Process

Due to low percentage of naproxen elimination, advance oxidation processes were selected to increase the efficiency of elimination. There are many oxidizing agent to study, such as O_3, Cl_2, performic acid. Table 2.5 revealed efficiency of naproxen removal of advance oxidation process. O_3 process was the most effective method to oxidize naproxen, but no further literature investigates about the toxic of O_3 reaction by products. For the Cl_2 process, their reaction was not complete oxidized, these substances were transformed to intermediate product not mineral. However their product affected to biofilm (Boyd, Zhang et al.,2005),it has a feasibility to impact to ecotoxicology.

Table 2.5 Efficiency of Removal Naproxen of Advance Oxidation Process.

Country	Type of oxidation process	Efficiency	Ref.
Japan	O_3	68-99.7	(Nakada et al.,2007)
Canada	O_3 Cl_2 Performic Acid	>95 36% <8	(Gagnon, et al.,2008)
USA	O_3 Cl_2 UV	>95 >80 >99	(Reclamation,2009)

2.6 Mesoporous Silicate

The Mesoporous silicates are the porous materials that were commonly used for adsorption process, because of their high surface area and high adsorption capacity. Classification of porous materials was based on pore size: macroporous > 50nm, mesoporous between 2nm and 50nm and microporous < 2nm. However, Mesoporous were mostly used due to suitable pore size range.

2.6.1 Synthesis of HMS(Haxagonal Mesoporous silicates) (Pinnavaia ; Tanev,and Pinnavaia,1996; Sevilla et al.,2004; Lin and Chen,2005)

HMS has been synthesized by the neutral template route (S^0I^0) that based on hydrogen bonding and self-assembly between neutral primary amine micelles (S^0) and neutral inorganic precursors (I^0). Moreover, template removal method of HMS was achieved either by calcination in air or solvent extraction.

2.6.2 Functionalization of HMS (Burleigh et al.,2001; Maria et al.,2004; Yu,2004)
There are two types of functionaliazation of ordered Mesoporous silicates.

Post-Synthetic Grafting

For post-synthetic grafting, the functional groups such as amino, mercapto and diamino were attached onto channel surface of Mesoporous silicate material. The disadvantages of grafting are hard to control the concentration and distribution of organic functional groups. However, it could preserve the mesostructure after modifying.

Co-condensation or Direct Synthesize

For direct synthesize, the functional groups were condensation with tetraethoxysilane (TEOS) in the presence of a surfactant template. The strong points of cocondensation method were homogeneous distribution and higher loading of organic functional groups. Nevertheless, after modifying method could loss original structure ordering. Table 2.6 showed comparison of post-synthetic grafting and direct synthesizes.

Table 2.6 Advantage and Disadvantage of Post-synthetic Grafting and Direct Synthesize

	Post Synthesis	Direct Synthesis
Advantage	• Good preservation of the mesostructure after post-modification.	• Simpler synthesis path • Shorter preparation time. • Better control and higher loading of organic functional groups. • Homogeneous distribution • Better stability of organic group
Disadvantage	• Hard to control the concentration and distribution of organic functional groups complicated and costly • Reduced pore size and pore volume • Limit of the functional groups loading. • Sometimes ineffective due to partial cross-linking of the functional groups with the silica-surface silanol groups	• Loss in original structure ordering such as aminopropyltriethoxysilane (APTES) functionalization.

2.7   Superparamagnetism

Magnetic materials divided into three types; Diamagnetic, Paramagnetic and Ferromagnetic.(Kailas ; Larson,2001-2010)

Diamagnetic: the materials have weak negative susceptibility when applied external field. This material could not preserve the magnetic properties after removing external field. The materials including copper, silver, and gold are diamagnetic at room temperature.

Paramagnetic: the materials have small positive susceptibility when applied external field. There is no net magnetization after removing external field. The materials including aluminum, calcium, titanium, alloys of copper.

Ferromagnetic: the materials have strong positive susceptibility when applied external field. This material could retain the magnetic properties after removing external field. It was classified in two class; antiferromagnetic and ferrimagnetic.

Antiferromagnetic materials such as Mn, Cr, MnO, NiO, CoO and MnCl2 showed zero magnetization due to dipole unpaired electrons line up opposite of one another.

Ferrimagnetic materials such as Ferrites and Magnetite displayed net magnetization because of unequal the opposing moments.

The superparamagnetic phenomena would occur with ferromagnetic materials that were smaller than 20-30 nm. The particle contained in single magnetic domain. When the temperature was higher than blocking temperature (T_B) in the Néel-Brown theory, the particle will act like paramagnetism that called superparamagnetism (Martien,1994; Fornara,2008; Dave and Gao,2009).

2.7.1 Application of Magnetic Nanoparticle (Deng et al.,2005; Gupta ,2005)

As a result of special properties, magnetic nanoparticle did not retain magnetization after the absence external field. Therefore, it can be used in biomedicine applications; magnetic resonance imaging (MRI), drug delivery, bio-separation,etc.

2.7.2 <u>Synthesis Magnetite Nanoparticle (Deng et al.,2005; Qu et al.,2010)</u>

Magnetite nanoparticle (Fe_3O_4) is a type of nanosized ferrimagnetic material, that have cubic inverse spinel structure. Magnetite can be used in many biomedicine applications due to their properties for example; superparamagnetic phenomena, high field irreversibility and high saturation field

2.7.3 <u>Coating Magnetite with Mesoporous Silicate (Vogt et al.,2010)</u>

In last decade, many researchers investigated about coating magnetite with many kinds of substances such as inorganic material, polymers and metal layers. However, silica is the most common material to coat magnetite due to their low toxicity, functionalize ability, large surface area and high bio-stability.

2.8 Adsorption Theory

2.8.1 <u>Adsorption Mechanism (Thommes ,2004)</u>

Adsorption is the inter-phase accumulation of substance on surface or interface. There are two types of adsorption mechanism; physical adsorption and chemical adsorption. The former was the attraction by relative weak forces, for example covalent, electrostatic, and Van der Waals force. This adsorption was normally reversible. For the latter, the chemical adsorption was strong interaction potentials that take placed by chemical bond between adsorbent and adsorbate. It was formed in monolayer and mostly irreversible. However, possible interaction forces between adsorbent and adsorbate are listed as followed:

- Vander waal forces: the attractive force between molecules depends on molecular weight.
- Hydrogen bonding: the strongly dipole force between hydrogen atom and electronegative atom such as oxygen and nitrogen.
- Covalent bonding: the chemical bond that shared pairs of electrons between atom and other covalent bonding.

- Electrostatic force: the force from opposite charges attraction. This force is the strongest force in intermolecular force.
- Hydrophobic force: the force that caused by hydrophobicity of surface and adsorbate which willing to form aggregation together better than to dissolve in water.

2.8.2 Adsorption Kinetic (Punyapalakul et al.,2009)

The adsorption kinetic can be applied to investigate the rate of adsorption depends on adsorption time. The obtained data also can be used to design contact time to complete equilibrium of adsorption. Two kinetic models including the pseudo-first order model and pseudo-second order model equations as well as intraparticle diffusion model will be investigated.

Pseudo-first-order Model

Pseudo-first-order model is general model to study reaction that depends on one reactant; the first order equation is given as (2.1):

$$\ln(q_e - q_t) = \ln q_e - k_1 t \tag{2.1}$$

Where q_e is the amount of solute adsorbed at equilibrium per unit weight of adsorbent (mg/ g), q_t is the amount of solute adsorbed at any time (mg/g) and k_1 is Pseudo first rate constant (1/h).

Pseudo-second-order Model

Pseudo-second-order model is mostly used model in chemical adsorption system; the second order equation is given as (2.2):

$$\frac{t}{q_t} = \frac{1}{k_2 q_e^2} + \frac{t}{q_e} \tag{2.2}$$

Where k_2 is Pseudo second rate constant (g/mg·h).

Intraparticle Diffusion

Intraparticle diffusion is commonly used model to describe mechanism adsorption; equation is given as (2.3):

$$q_t = k_{id}t^{\frac{1}{2}} + C \tag{2.3}$$

Where k_{id} is the intraparticle rate constant(mg/g·min$^{1/2}$) and C is the thickness boundary layer.

There are three step of adsorption mechanism:

(1) Film Diffusion – mass transfer go through to boundary layer of adsorbents

(2) Intrapraticle Diffusion – adsorbate pass through the pore of adsorbents

(3) Equilibrium Stage –the step that the rate of intraparticle diffusion is constant

2.8.3 Adsorption Isotherm (Özer et al.,2006; Han et al.,2009; Akpa and Unuabonah,2011)

The objective of the adsorption kinetic is to investigate maximum adsorption capacity that associate with equilibrium concentration of the residue of adsorbate. The isotherm was studied in four isotherm models.

Langmuir Isotherm

The Langmuir isotherm is general isotherm to study about monolayer and homogenous surface adsorption. The equation is given as (2.4):

$$q_e = \frac{q_m K_L c_e}{1 + K_L c_e} \tag{2.4}$$

Where q_e is the amount of solute adsorbed at equilibrium per unit weight of adsorbent (mg/ g), q_m is the amount of solute adsorbed in complete layer (mg/g) and K_L is a Langmuir constant related to the affinity of the binding sites and energy of adsorption (L/mg)

Freundlish Isotherm

The Fruendlish isotherm is common used in aqueous solution for multilayer and heterogeneous surfaces adsorption. The equation is given as (2.5):

$$q_e = K_F c_e^{1/n} \qquad (2.5)$$

Where K_F is a Freundlish constant related to the adsorption capacity and adsorption intensity of the sorbent and 1/n is Freundlish intensity parameter.

Redlich-Peterson Isotherm

The Redlich-Peterson isotherm is improved over Freundlish and Langmuir isotherm. It is applied to describe wide range isotherm. This isotherm contains three parameters to describe an empirical isotherm. The equation is given as (2.6):

$$q_e = \frac{AC_e}{1+BC_e^g} \qquad (2.6)$$

Where A, B and g are the Redlich–Peterson parameters, g lies between 0 and 1. When g=1, this equation converts to Langmuir equation.

Sip Isotherm

The Sip isotherm is union between Freundlish and Langmuir isotherm. It is expected to predict heterogeneous surface adsorption. Raising concentration of adsorbate will join together with Freundlish isotherm. The equation is described as (2.7)

$$q_e = \frac{q_m (b_s C_e)^{n_s}}{1+ (b_s C_e)^{n_s}} \qquad (2.7)$$

Where q_m is the monolayer adsorption capacity (mg/g), b_s is a Langmuir constant, n_s is Freundlish parameter.

2.9 Adsorbent separation

2.9.1 Filtration Theory (Moorthy,2007; Agency,2010; Lortragool,2010)

The principle mechanism of transportation filtration consists of three processes: interception, diffusion and gravitational deposition.

Interception : The direct interception occurs when the particles pass closely in the filter fiber and if the radius of the particle is larger than the gap between the flow streamline and the fiber, the particles are captured. The equation of interception efficiency is demonstrated as (2.9).

$$\eta_{int} = \frac{3}{2}\left[\frac{d_p}{d_m}\right]^2 \tag{2.9}$$

Where d_m is media diameter (m) and d_p is diameter of adsorbent particle (m).

Diffusion : For small particles less than 0.1μm diameter, the particles are capture when the particles randomly move. The equation of diffusion efficiency is given by (2.10).

$$\eta_{Diff} = 0.9\left[\frac{KT}{\mu_c d_p d_m v_0}\right]^{\frac{2}{3}} \tag{2.10}$$

Where K is Boltzmann's constant $(1.38 \times 10^{-23}$ kg·m^2/K·s^2), T is absolute temperature (K), μ_c is viscosity of solution (kg/(m·s)) and v_0 is velocity rate (m/s).

Gravitation Deposition : The particles settle out by influence of gravity. The sedimentation efficiency is defined as (2.11).

$$\eta_{sed} = \frac{w}{v_0} = \frac{\Delta\rho g d_p^2}{18\mu_c v_0} \tag{2.11}$$

Where w is velocity rate of floating (m/s), $\Delta\rho$ is difference of media and adsorbent particle density (g/cm^3) and g is gravity accelerate (m/s^2).

Hence, all mechanism is summarized to total efficiency of transportation that defined as (2.12).

$$\eta_T = \eta_{int} + \eta_{Diff} + \eta_{sed} \qquad (2.12.1)$$

$$\eta_T = \frac{3}{2}\left[\frac{d_p}{d_m}\right]^2 + 0.9\left[\frac{KT}{\mu_c d_p d_m v_0}\right]^{\frac{2}{3}} + \frac{\Delta\rho g d_p^2}{18\mu_c v_0} \qquad (2.12.2)$$

When the solution flows through the media filter, there are some adsorbent particles that were trapped on media. These adsorbent particles that were captured by media per particle are assumed as x in eq. (2.13):

$$\eta_T = \frac{x}{\frac{v_0 C \pi d_m^2}{4}} \qquad (2.13.1)$$

$$x = \eta_T \frac{v_0 \pi C d_m^2}{4} \qquad (2.13.2)$$

Where C is concentration adsorbent (mg/L).

For depth of media filter, the total of captured adsorbent particles that denoted as x_T is derived in (2.14).

$$x_T = x \frac{A_0 dH(1-\varepsilon)}{\pi d_m^3/6} \qquad (2.14)$$

Where A_0 is cross section area (m^2), H is depth of media filter (m) and ε is porosity of media filter.

To assume α is the collision efficiency, the collided adsorbent particles that denoted as x_c is defined as (2.15).

$$x_c = \alpha x \frac{A_0 dH(1-\varepsilon)}{\pi d_m^3/6} \qquad (2.15)$$

From eq. 13, the collided adsorbent particle is equal the quantity of removal adsorbent solution that is given by (2.16).

$$-v_0 A_0 dC = \frac{3}{2}\alpha\eta_T \frac{A_0 v_0 C(1-\varepsilon)dH}{d_m} \qquad (2.16.1)$$

$$\frac{dC}{C} = -\frac{3}{2}(1-\varepsilon)\alpha\eta_T \frac{dH}{d_m} \qquad (2.16.2)$$

$$ln\frac{C_S}{C_0} = -\frac{3}{2}(1-\varepsilon)\alpha\eta_T \frac{H}{d_m} \qquad (2.16.3)$$

Finally, the filtration efficiency was calculated by (2.17).

$$1 - \frac{C_S}{C_0} = 1 - e^{-\frac{3}{2}(1-\varepsilon)\alpha\eta_T\frac{H}{d_m}} \qquad (2.17)$$

Where C_s is output concentration (mg/L) and C_o is input concentration(mg/L)

2.9.2 HGMS Filter

In last decade, HGMS filter is commonly used in magnetic filtration that separate magnetic materials from non-magnetic solution. The mechanism of magnetic filtration is to handle the magnetic particles in magnetic filter media such as stainless steel that induced by the magnetic field. There are three methods to generate external magnetic field; permanent magnet (Sato,2004), electromagnetic solenoid (Ditsch et al.,2005) and superconducting magnet (Mitsuhashi et al.,2003; Laboratory,2004; Baik et al.,2010). Commonly, permanent magnet is easy to operate and low cost to. Nevertheless, the magnetic flux density is limited at less than 1 T and difficult to control magnetic field density. For electromagnetic solenoid method, the magnetic field is created by a solenoid electrical conduction wires. This process also has limitation of magnetic field at less than 2.4 T. Superconducting magnet is new technique to generate high magnetic flux density. It is constructed by permitting electrical power input to the coil of superconducting wire at low temperature under superconductivity temperature.

2.9.3 Theory of Magnetic Separation

Magnetic Strength Field (H)

The magnetic strength field is the quantity of magnetizing force that generated to magnetic material by current.

Magnetic Flux Density(B)

The magnetic flux density is the amount of internal magnetizing force that magnetic materials such as permanent magnet provide the magnetic force. Magnetic strength field is depending on the magnetic permeability of material and magnetic strength field, the equation is shown as (2.18).

$$B = \mu_m H \tag{2.18}$$

Where H is magnetic strength field (A/M), B is magnetic flux density (T or Wb/m^2) and μ_m is magnetic permeability of material (Wb/(A·m))

Magnetic Force

The magnetic force is the force of moving charge that defines in the Lorentz Law; the equation is given as (2.19).

$$F_m = q(v \times B) \tag{2.19}$$

Where F_m is magnetic force (N), q is the electric charge of the particle (C), v is the instantaneous velocity of the particle (m/s), and B is the magnetic field (T).

Moreover, magnetic force of particle when applies the magnetic field express as (2.20).

$$F_m = \mu_0 V_p M_p \cdot \nabla H \tag{2.20}$$

Where F_m is magnetic force of particle, μ_0 is magnetic permeability of vacuum (Wb/(A·m)), V_p is particle volume(m^3), M_p is the particle magnetization (A/m) and ∇H is the gradient of magnetic strength field at the position of the particle.

Moreover, there are three forces that involved in magnetic filtration process.

Gravitational Force

The gravitational force is the force that drags the particles to fall down in the fluid by their own weight due to gravity; the equation is expressed as (2.21).

$$F_g = (\rho_p - \rho_g)V_p g \qquad (2.21)$$

Where F_g is gravitational force (N), ρ_p is density of particle (kg/m^3), ρ_g is density of fluid (kg/m^3) and V_p is gravitational acceleration (m/s^2).

Centrifugal Force

The centrifugal force is the movement force that occurs when the particle is agitated, the equation is express as (2.22).

$$F_c = (\rho_p - \rho_g)\omega V_p r \qquad (2.22)$$

Where F_c is centrifugal force (N), ω is the angular velocity (rad/s) and r is the radial of the particle (m).

Drag Force

The drag force is the frictional force of particle react to gravity force, now known as Stoke's law. The equation is shown as (2.23).

$$F_d = 3\pi\eta d_p(v_{f-}v_p) \qquad (2.23)$$

Where F_d is drag force (N), η is the dynamic viscosity of fluid (N·s/m^2) and d_p is the diameter of the particle (m).

2.10 Breakthrough Curve Theory (Samuel D. ,1987)

Bed Depth Service Time (BDST) is the theory that proved by Bohart and Adams. The model investigates that the adsorption rate is proportional to the residue adsorbent capacity and adsorbed pollutant concentration. The equation is expressed as (2.24).

$$\ln\left(\frac{C_0}{C_B}\right) = \ln[exp(KN_0D/V) - 1] - KC_0t \qquad (2.24)$$

Where t is time at breakthrough (hr.), V is linear flow rate (cm/hr), D is bed depth of adsorbent (cm), K is rate constant (L/(mg·hr)), N_0 is adsorption capacity (g/cm^3), C_0 is influent solute concentration (g/L) and C_B is solute concentration at breakthrough (g/L).

This equation is rearranged to linear function by plotting between bed depth and time at breakthrough point under controlling constant flow rate and initial concentration that given as (2.25). The bed depth is examined by this equation for finding breakthrough time. The slope and intercept of this equation is shown as (2.26), (2.27).

$$t = \frac{N_0}{C_0V}\left[D - \frac{V}{KN_0}\ln\left(\frac{C_0}{C_B} - 1\right)\right] \qquad (2.25)$$

$$a = \frac{N_0}{C_0V} \qquad (2.26)$$

$$b = \frac{1}{C_0K}\ln\left(\frac{C_0}{C_B} - 1\right) \qquad (2.27)$$

To design different flow rate, the factor is inserted to correlation equation that summarized as (2.28). The slope of this equation is shown as (2.29).

$$t = a'x + b \qquad (2.28)$$

$$a' = \frac{V \cdot a}{V'} \qquad (2.29)$$

Where t is time at breakthrough (hr), x is bed depth (cm), a is old slope, a' is new slope, b is ordinate intercept.

To design different influent solute concentration, the factor is inserted to correlation equation that summarized as (2.30). The slope and intercept of equation is expressed as (2.31) and (2.32).

$$t = a'x + b' \qquad\qquad (2.30)$$

$$a' = \frac{C_0 \cdot a}{C_1} \qquad\qquad (2.31)$$

$$b' = b \left(\frac{C_0}{C_1}\right) \frac{\ln[(C_1/C_F)-1]}{\ln[(C_0/C_B)-1]} \qquad\qquad (2.32)$$

Where t is time at breakthrough (hr), x is bed depth (cm), a is old slope, a' is new slope, b is ordinate intercept, b and b' are old and new intercept, C_0 and C_1 are old and new influent solute concentration (g/L) and C_B and C_F are old and new effluent solute concentration (g/L).

2.11 Literature Reviews

2.11.1 Adsorption of Pharmaceutical

Yu et al. (2008) studied adsorption characteristic of pharmaceutical residues and endocrine disrupting compound; Naproxen, carbamazepine and nonylphenol on activated carbon that had 1030 and 1156 m^2/g of surface area at low concentration ranges. They found that log K_{ow} influenced to adsorption affinity of micro pollutants; a higher log K_{ow} had higher adsorption capacity.

Eduardo et al. (2010) investigated adsorption of naproxen and ketoprofen on carbon blacks by vary temperature, ionic strength, surface area, pore volume and pH. This study discovered all factors were affect on adsorption of naproxen, a higher temperature would stronger the interaction between the solute and adsorbent. The electrostatic force effects on adsorption of naproxen.

Tung et al. (2009) reported that pharmaceuticals; carbamazepine, clofibric acid, diclofenac, ibuprofen and ketoprofen on mesoporous silicate SBA-15 had high adsorption capacity except for clofibric acid. Adsorptions of five pharmaceuticals were pseudo-

second-order kinetic and fitted for Freundlich isotherm model. Hydrophilic interaction influenced mechanisms of their adsorption.

Sindia et al. (2008) compared adsorption capacities naproxen of mesoporous silicates, modified mesoporous silicates and activated carbon in $\mu mol/m^2$ unit. They modified Mobile Crystalline Material (MCM-41) by functionalized with Ni and amino group that denoted as NiCl2_dm_MCM-41 and NiNH2_g_MCM-41. The BET surface area of activated carbon, NiNH2_g_MCM-41, NiCl2_dm_MCM-41 and pristine MCM-41 were 1030 m^2/g, 40 m^2/g, 600 m^2/g and 1198 m^2/g, respectively. The adsorption capacities followed: activated carbon (0.67) > NiNH2_g_MCM-41 (0.42) > NiCl2_dm_MCM-41 (0.03) > pristine MCM-41 (0.01) at 18 mg/L initial concentration of naproxen. The result showed that functional group was important factor of adsorption and functionalization of adsorbent decreased their surface area.

Punyapalakul et al. (2004) studied effect of surface functional groups on the adsorption of dichloroacetic acid (DCAA) by hexagonal mesoporous silicate (HMS). There are three surface functional groups; alkyl-, amino-, and mercapto- groups denoted as OD-HMS, AM-HMS, and M-HMS. They found that AM-HMS highly adsorbed DCAA with strong charge due to the hydrophobicity. Beside, bi-functional group between mercapto functional group and amino functional group can enhance adsorption capacity because of higher active surface site and demonstrated higher adsorption capacity than AM-HMS.

There are many researches who investigated new technique to encapsulated magnetic material in mesoporous silicate, this magnetic property are supposed to enhance separation efficiency by HGMS filter. **Hua et al.** (2003) synthesized the magnetic HMS by encapsulated mesoporous material in magnetite denoted as HMS-SP. Obtained HMS-SP was investigated DDT adsorption capacity and magnetic separation efficiency from aqueous phase. They reported that HMS-SP had high DDT adsorption capacity and significant effective separation from aqueous solution.

From previous studies, adsorption process has high possibility to be applied for naproxen removal from wastewater. Although, studied carbon based adsorbents reported by previous researches had high adsorption capacity, however, selectivity of target compounds of carbon based adsorbents were suggested to be low due to their low uniformity of surface structure. Mesoporous silicate materials such as MCM-41 and HMS have been developed to enhance adsorption capacity of micro-pollutants. The advantages of these materials are uniform pore size of distribution and surface functional groups which can enhance selective adsorption capacity. Moreover, these porous silicate materials can be enhanced separation efficiency by magnetic separation processes due to their modified superparamagnetic characteristic.

2.11.2 Application of HGMS Filter

Previous studies have investigated particle separation efficiency by magnetic filtration. The configuration of equipment was set external magnetic flux density and equipped direction of magnetic field to opposite with fluid flow. Magnetic filter was inserted inside the column under set magnetic field.

Mitsuhashi et al. (2003) investigated magnetic filter application to separate Fe_3O_4 modified with octadecyl group that adsorb nonylphenol and Bisphenol A from wastewater. The austenitic stainless steel sheets were used as magnetic filter to capture the magnetic particle and generated 1-1.7 T by superconducting magnet. The experiment conditions are; flow rate: 20 liter / min, magnetic filter passage: 10 min and amount of adsorbent: 490 and 1100 mg/L. For this process, Fe_3O_4 which adsorbed nonylphenol and bisphenol A can be removed from wastewater flow effectively.

Ditsch et al. (2005) studied the effect of column length, velocity, and magnetic particle size on HGMS filtration. The experiment is varied: column length: 3.5 and 10.5 cm, velocity: 0.3,0.6,1,2,3 and 4 cm/s and magnetic particle size: 80,110 and 140 nm but controlled 0.16 of packing fraction, 0.5% wt particle concentration and 0.5M NaCl of ionic strength. For this model, 1.3 T the intensity of magnetic was created by

electromagnet and stainless steel wires were used to magnetic filter. The result of this study showed that longer length column, bigger particles, slower velocity enhanced the capture efficiency and the cluster bigger than 50 nm had more than 99.9% of the efficiency at high flow rate.

Waynert et al. (2004) investigated removal of heavy metal; Zn, Cu, Pb, Cd, Ag, Fe and Mn by HGMS filter. Applied HGMS filter system was used 2.0 T superconducting magnet and ferromagnetic filter. The ferrite feeding that reacted with heavy metals was captured by filter. Obtained results showed that flow rate and magnetic flux density effect on efficiency of system.

From previous researches, it can be concluded that magnetic filtration by permanent magnets can be applied to separate superparamagnetic particles from aqueous flow, especially concerning about material and operation cost. However, it has a limitation about magnetic flux density that might decrease separation efficiency comparing with electromagnetic and superconducting magnets.

2.11.3 BDST Model

Zou et al. (2011) studied adsorption of uranium (VI) on zeolite by continuous fixed bed depth. They found that extending bed depth performed steeper slope and higher surface area to adsorb due to increasing mass of adsorbent. Moreover, breakthrough curve was lower slope causing by slower flow rate. They reported that it was more breakthrough time when inlet concentration is small. The experiment data was apply with BDST for predict breakthrough time. The result of BDST was related to experiment data.

Han et al. (2009) investigated breakthrough curve of continuous fixed bed column. Phoenix tree leaf powder was used fixed bed to remove methylene blue. The experiment indicated that increasing breakthrough time related to decreasing flow rate, influent adsorbate concentration and longer fixed bed depth. The result were discussed in four model; Thomas, Adam-Bohart, Yoon-Nelson and Clark. In case of Adam-Bohart model, the correlation coefficients is higher than 0.9, so this model was successful to apply this

model. Beside, predicted breakthrough time by BDST model was slightly different from experimental breakthrough time.

In conclusion, effects of bed depth, flow rate and initial concentration of pollutant influence breakthrough curve including breakthrough time and slope of curve due to surface area and contact time. BDST model was most used to predict breakthrough time in different flow rate and initial particle concentration. However, application of BDST model on HGMS filter still has not been reported yet.

CHAPTER III

MATERIALS AND METHODS

3.1 Materials

3.1.1 Chemical Reagents

1.	Dodecylamine	98%	ACROS ORGANICS
2.	Tetraethoxysilane	98%	ACROS ORGANICS
3.	3-aminopropyltriethoxysilane	>98%	Fluka
4.	3-mercaptopropyltrimethoxysilane	>98%	Fluka
5.	Powdered activated carbon		ShirasakiS-10 Japan enviroChemicals, Ltd.
6.	Ethyl alcohol absolute	RPE-ACS	CARLO ERBA
7.	Sodium hydroxide	AR grade	LAB SCAN
8.	Hydrochloric acid	37%	CARLO ERBA
9.	Sulfuric acid	98%	LAB SCAN
10.	Potassium dihydrogenphosphate	AR grade	Riedel-de-Haen
11.	Dipotassium hydrogenphosphate	AR grade	Riedel-de-Haen
12.	Naproxen	98%	Sigma-Aldrich.
13.	Iron (II) chloride tetrahydrate	99%	Sigma Aldrich
14.	Iron (III) chloride hexahydrate	96%	Ajax Finechem
15.	Ammonium hydroxide	28-30%	J.T. Baker
16.	Sodium chloride	99%	LAB SCAN

3.1.2 Instruments

1. Fourier transform Infrared Spectroscopy: Perkin Elmer, Spectrum one
2. UV- vis spectrophotometer: GENESYS 10SUV-VIS with 1 and 5- cm quartz cells
3. Shaker: Green SSriker II
4. Inductively coupled plasma atomic emission spectroscopy (ICP-AES): LECO,corporation)
5. Zeta-Meter: Zeta-Meter System 3.0, Zeta-Meter Inc.
6. Magnetic stirrer : AS ONE Rexim RS 6D model
7. Scanning Electron Microscope (SEM): JSM -6400
8. pH meter: Mettler-Toledo AG, CH-8902 Urdorf
9. Tensiometer: A Dataphysics DCAT-11 tensiometer

3.2 Experimental Procedure

3.2.1 Synthesis of Adsorbents

Synthesis of Fe_3O_4 Particle (Qu et al.,2010)

Fe_3O_4 was prepared by this following method: 0.046 mol of $FeCl_3 \cdot 6H2O$ and 0.223 mol of $FeCl_2 \cdot 4H_2O$ were mixed into 150 mL of DI water under vigorous stirring. After that add 20mL of Ammonium Hydroxide 25%. After the mixture was stirred for 30 min, added 3mL of Oleic acid. Then, the mixture was heated to 75°C for 1hr. Finally, the product was washed and separated by magnet with DI water and ethanol in three times, and then dried. The Fe_3O_4 was obtained.

Synthesis of Coated Hexagonal Mesoporous Silicates(HMSs)(Tian et al.,2009)
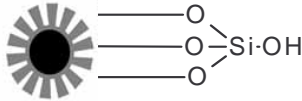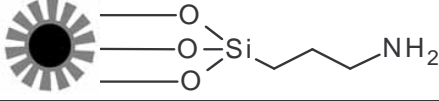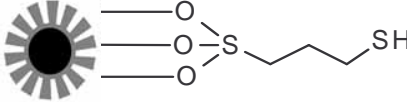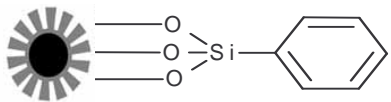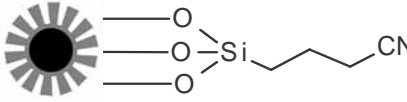
HMS-SP was prepared by this following method: 0.5g of obtained Fe_3O_4 was dispersed in 250mL of 0.1M HCl. After that washed with DI water and separated by magnetic separation. The mixture of 3.94 g of ethanol and 27.36 g of H_2O were added in to washed Fe_3O_4 and then mixed in vigorous stirring for 30 min. Under stirring, 2g of tetraethylorthosilicate (TEOS) was added in to the mixture and the mixture was stirred

and age at ambient temperature for 20 hr. Then the product was separated by magnet and washed with DI water and ethanol. After that, the template removal was carried out by refluxing in 200mL ethanol at 80°C for 10 hr, and duplicates refluxing.

Functionalized Group by Co-condensation (Punyapalakul et al.,2009)

Functionalized group by co-condensation was prepared by these following methods: 0.5g of Fe_3O_4 was dispersed in 250mL of 0.1M HCl. After that washed with DI water and separated by magnetic separation. The mixture of 3.94 g of ethanol and 27.36 g of H_2O were added in to washed Fe_3O_4 and then mixed in vigorous stirring for 30 min. Under stirring, 2g of tetraethylorthosilicate (TEOS) was added. After 30 min, the 0.25 mol of each organosilane (such as of 3-aminopropyltriethoxysilane (APTES), 3-mercaptopropyltriethoxysilane (MPTMS), phenyltrimethoxysilane and 4-(triethoxysilyl)butyronitrile was added to the mixture, and then vigorous stirring and age at ambient temperature for 20 hr. Then the obtain particle was separated by magnet and washed with DI water and ethanol. After that, the template removal was carried out by refluxing in 200mL ethanol at 80°C for 10 hr, and duplicates refluxing. Finally, A-HMS-SP, M-HMS-SP, P-HMS-SP and N-HMS-SP will be obtained, respectively. Table 3.1 shows surface functional groups structures of each adsorbent.

Table 3.1 Surface Functional Groups Structure of Synthesized Adsorbents

Adsorbents	Chemical structures	Functional groups
HMS-SP		Silanol (SiOH)
A-HMS-SP		Amino (NH_2) Silanol (SiOH)
M-HMS-SP		Mercapto (SH) Silanol (SiOH)
P-HMS-SP		Phenyl Silanol(SiOH)
N-HMS-SP		Nitrile (CN) Silanol (SiOH)

3.2.2 Physico-chemical Characterization of Adsorbents

The synthesized adsorbents will be measured their physico-chemical properties by various methods that expressed as Table 3.2. All of characteristic parameters will be used to discuss about adsorption mechanisms of NAX on the materials.

Table 3.2 Physico-chemical Characteristic Parameters and Measurement Method

Parameters	Instrument/Analysis
Surface area and pore size	BET/Nitrogen Adsorption
Surface functional group	Fourier transform Infrared Spectroscopy (FT-IR)
Sulfur content	ICP-AES
Surface charge	Zeta potential analyzer
Surface structure	Scanning Electron Microscopy (SEM)

Surface Area and Pore Size

Surface area and pore size of synthesized adsorbents were analyzed by using data from nitrogen adsorption isotherm derived by BET isotherm. The BET isotherm was found by Brunauer, Emmett and Telleris. It was general isotherm that used to determine adsorption phenomena under 77K. Moreover, this application can identify pore size and surface area of adsorbent. The equation is shown in (3.1). BET isotherm was the physical gas adsorption isotherm that adsorbed inert gas commonly nitrogen on solid material.

$$\frac{1}{v\left[\left(\frac{P_0}{P}\right)-1\right]} = \frac{c-1}{v_m c}\left(\frac{P}{P_0}\right) + \frac{1}{v_m c} \tag{3.1}$$

Where P and P_0 are equilibrium and saturation pressure of adsorbent, v and vm are adsorbed and monolayer adsorbed gas and c is BET constant.

Surface Functional Group

Surface functional groups of functionalized adsorbents and pristine adsorbent were determined by Fourier Transform Infrared (FT-IR). The organo silane functional groups were defined by band of chemical bonding at wavenumber between 400 and 4000 cm^{-1}.

Sulfur Content

Quantity of sulfur was examined by sulfur determinator model SC-132. The sample was heat at 400°C. The sulfur content was measure existence of SO_2.

Surface Charge

Zeta potential meter were used to measure surface charge. 0.005g of adsorbents were mixed in pH solution in range 3 to 10 under controlled 0.01M ionic strength by phosphate buffer for 24 hours. After that mixtures were analyzed and the results were plot between voltage of surface charge and pH values.

Surface Structure

Scanning electron microscope (SEM) was used to consider surface structure of synthesized adsorbents including uniform size distribution of particle.

3.2.3   Adsorption Study

Adsorption Kinetic

1) Added 0.200 g of each adsorbents into Erlenmeyer flask.
2) Poured 150 mL of 5 mg/L NAX solution and control pH7 and IS 0.01 M by using phosphate buffer.
3) Shaked Erlenmeyer flask in temperature at 25 ± 2 °C until 24 hours.
4) Collected sample and filtrate the sample through GF/C filter paper at 0,1,3,5,10,15,30,60,180,360,540,720,1440 min.
5) Measured filtrated sample by UV-visible spectrophotometer at 230 nm.

Adsorption Isotherm

1) Added 0.020 g adsorbent into Erlenmeyer flask.
2) Poured 15 mL of NAX solution in range 0.5-10 mg/L and controlling under pH7 and 0.01 M by using phosphate buffer.
3) Shaked Erlenmeyer flask in temperature at 25 ± 2 °C until 24 hours.
4) Collected sample and filtrating the sample through GF/C filter paper.
5) Measured filtrated sample by UV-visible spectrophotometer at 230 nm.
6) Repeated all process with changing controlled pH at 5 and 9 by phosphate buffer.

Hydrogen Bonding Measurement between NAX and HMS-SP Surface.

1) Added 0.100 g of HMS into Erlenmeyer flask.

2) Poured 30 mL of NAX in hexane.

3) Shaked Erlenmeyer flask in temperature at 25 ± 2 °C until 24 hours.

4) Collected sample and filtrating the sample through GF/C filter paper.

5) Dried filtrated HMS in the oven at 105°C for 24 hour.

6) Analyzed NAX adsorbed HMS in hexane by FT-IR.

7) Compared between the result of NAX adsorbed HMS in hexane and virgin hexane.

3.2.4   High Gradient Magnetic Separate Filtration

The magnetic filtration system consisted of wire stainless steel filter, 3 acrylic pipe diameter 0.8 cm and height 5 cm, pair of permanent magnets and peristaltic pump that show as Figure 3.1. The gap between permanent magnets was 3 cm.
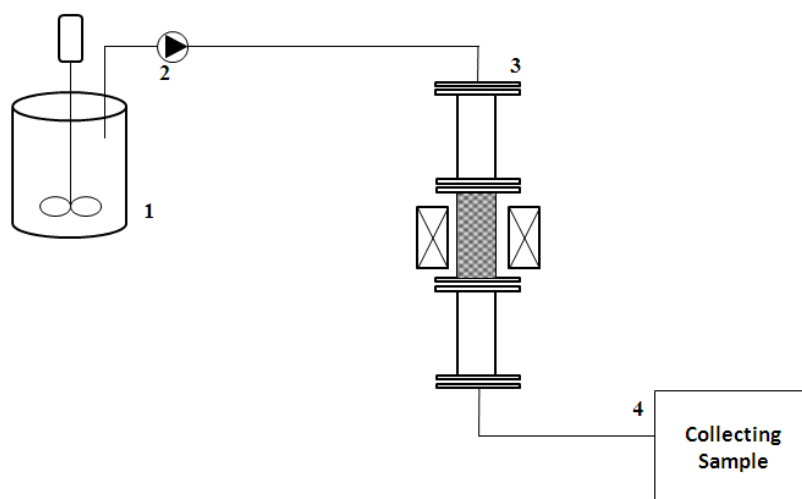
Figure 3.1 System Filtration Process; Stirrer (1), Peristaltic Pump (2), Magnetic Filtration (3) and Collecting Sample (4).

Effect of Flow Rate

1) Mixed synthesized adsorbent that performed the highest adsorption capacity with DI water in ratio 0.5 g of adsorbent per 1 Liter of DI water.

2) Pumped the mixture to the filter at varied flow rate from 0.75 to 1.5 cm/min.

3) Collected the sample until breakthrough point.

4) Measured the concentration of adsorbent by turbidity meter.

The condition of this experiment were summarized in Table 3.3

Table 3.3   The Parameters of HGMS Filter for Study Effect of Flow Rate

Parameters	Values
Varied parameters	
• Flow rate	0.75, 0.95 and 1.25 cm/min
Controlled parameters	
• Depth filter	5 cm
• Surface area filter	37.23 cm^2
• Particle concentration	0.5g/L

Effect of Depth Filter

To study effect of depth filter, experiment was conducted as same as previous study of effect of flow rate, but the flow rate was fixed as well as concentration of adsorbent. The depth filter was varied by 1.5, 3 and 5 cm.

The condition of this experiment were summarized in Table 3.4

Table 3.4 The Parameters of HGMS Filter for Study Effect of Depth Filter

Parameters	Values
Varied parameters	
• Depth filter	1.5,3 and 5 cm
Controlled parameters	
• Flow rate	0.95 cm/min
• Surface area	37.23 cm^2
• Particle concentration	0.5g/L

Effect of Surface Area of Stainless Filter

To investigate effect of filter surface, filtration experiment was conducted as same as previous study of effect of flow rate, but controlled flow rate, and magnetic flux density. Surface area of the filter was varied from 19 to 50 cm^2.

The condition of this experiment were summarized in Table 3.5

Table 3.5 The Parameters of HGMS Filter for Effect of Surface area Filter

Parameters	Values
Varied parameters	
• Surface area filter	37.23 cm^2
Controlled parameters	
• Flow rate	0.95 cm/min
• Depth filter	5 cm
• Particle concentration	0.5g/L

Effect of Concentration of Synthesized Adsorbent Particle.

To investigate effect of adsorbent concentration, filtration experiment was conducted as same as previous study of effect of flow rate, but controlled flow rate, and magnetic flux density. The concentration of adsorbents was varied from 0.3 to 1 g/L.

The condition of this experiment were summarized in Table 3.6

Table 3.6 The Parameters of HGMS Filter for Study Effect of Adsorbent Concentration.

Parameters	Values
Varied parameters	
• Particle concentration	0.3,0.5 and 1g/L
Controlled parameters	
• Flow rate	0.95 cm/min
• Surface area filter	37.23 cm^2
• Depth filter	5 cm

Effect of NAX in Filtration Efficiency

To evaluate removal efficiency of NAX from synthetic wastewater by adsorption on synthesized adsorbent and separated by HGMS filter, the filter conditions were fixed by parameters that performed the highest filtration efficiency: flow rate, filter depth, surface area of filterand adsorbent concentration. The concentration of NAX in synthetic wastewater was set at 5 mg/L. Moreover, filtration under above conditions was conducted without magnetic flux density in order to evaluate effect of magnetic field on filtration efficiency. Experimental procedure can be concluded as following:

1) Mix selected adsorbent with 5 mg/L NAX solution in ratio of 0.5 g adsorbent per 1 Liter of solution under controlled pH 7, IS 0.01M and temperature at $25 \pm 2°$C until equilibrium state.
2) Pump the mixture to the filter.

3) Collect the sample until breakthrough point.

4) Measure the concentration of adsorbent by turbidity meter.

5) Measure residual concentration of NAX from the output of HGMS filter.

The condition of this experiment are summarized in Table 3.7

Table 3.7 The Parameters of HGMS Filter for Study Effect of NAX

Controlled parameters	Values
• Depth filter	5 cm
• Surface area filter	37.23 cm^2
• Particle concentration	0.5g/L
• Flow rate	0.95 cm/min

CHAPTER IV

RESULTS AND DISCUSSION

4.1 Characteristic for Physical –chemical Properties of Synthesized Adsorbents

All synthesized adsorbents were characterized physico-chemical characteristics such as surface area, pore size, surface functional group, surface charge, hydrophobicity and particle size.

4.1.1 Surface Area and Pore Size

BET isotherm was the physical gas adsorption isotherm that adsorbed inert gas commonly nitrogen on solid material. The process will occurred in multilayer. This method would analyze surface area and pore size of HMS-SP modified with organic functional groups (A-HMS-SP, M-HMS-SP, P-HMS-SP and N-HMS-SP) by using nitrogen adsorption.

Nitrogen adsorption-desorption isotherm of all adsorbents are shown in Figure 4.1. Physico-chemical characteristics of synthesized adsorbents were summarized in Table 4.1. For A-HMS-SP, surface structures of functional group grafted adsorbent were changed significantly from pristine HMS-SP by decreasing surface area and increasing pore diameter due to the collapse of silicate porous structure. Surface areas of M-HMS-SP, N-HMS-SP and P-HMS-SP were decreased a little bit comparing with pristine HMS-SP. However, PAC has the highest surface area than others adsorbents. Pore size diameters of all adsorbents except PAC were in range 2-50 nm which can identify mesoporous silicate structure.
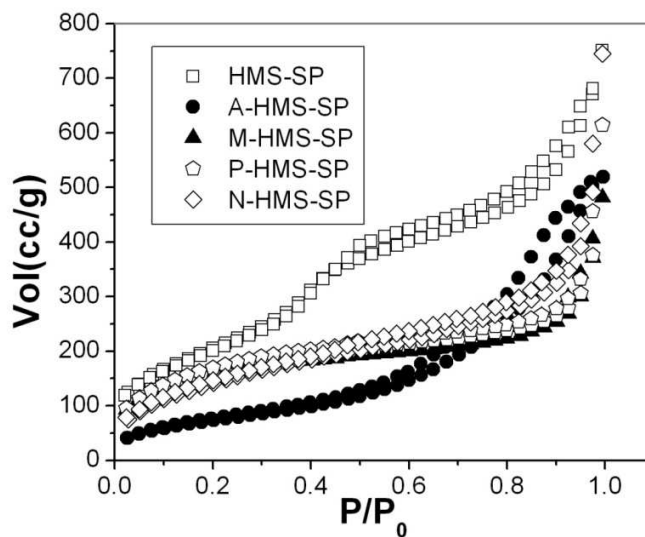
Figure 4.1 Nitrogen Adsorption–desorption Isotherms and Surface Charge of A-HMS-
SP, M-HMS-SP, HMS-SP, N-HMS-SP and P-HMS-SP.

Table 4.1   Physico-chemical Characteristics of Synthesized Adsorbents.

Adsorbents	Pore diameter (nm)	BET Surface area (m^2/g)	pH$_{zpc}$	Surface functional groups	Hydrophobicity
A-HMS-SP	11.81	272	8.8	Amino	Hydrophilic
M-HMS-SP	5.34	558	6.2	Mercapto	Hydrophobic
HMS-SP	6.02	771	4.4	Silanol	Hydrophilic
P-HMS-SP	6.42	592	5.6	Phenyl	Hydrophobic
N-HMS-SP	8.63	534	4.5	Nitrile	Hydrophobic
PAC[a]	1.90	980	9.5	Carboxyl Phenyl Others	Hydrophobic

[a](Punyapalakul et al, 2009)

4.1.2 Content of Sulfur

Content of sulfur was measure by Inductively Coupled Plasma Atomic Emission Spectroscopy (ICP-AES). The result found that M-HMS-SP had 5.57% by weight of sulfur, which represents mercapto functional group (-SH).

4.1.3 Surface Functional Groups

Surface functional groups of all synthesized adsorbents were determined by Fourier Transform Infrared (FT-IR). According to Figure 4.2, FT-IR cannot detect band of O-H free bonding that used to identify silanol group at wavenumber of 3746 cm^{-1} on pristine HMS-SP. However, board peak at 3433 cm^{-1} can identify hydrogen bonding which might caused by interaction between water and silanol group on HMS-SP surface. For amino and mercapto functional group, band of N-H bonding and S-H bonding cannot be detected at wavenumber of 3300 – 3400 cm^{-1} and 2560 cm^{-1}, respectively, due to low mass loading. But grafted organo-functional groups can be confirmed by represented C-H bonding at wavenumber of 2890-2960 cm^{-1} of A-HMS-SP and M-HMS-SP. Moreover, sulfur intensity value measured by ICP-AES can support the existence of mercapto functional group on M-HNS-SP surface. In case of phenyl group in P-HMS-SP, it was found C-H bonding, C=C bonding of aromatic ring and benzene band at 2890-2960 cm^{-1}, 1434 cm^{-1} and 705 cm^{-1}. To determine cyanide functional group, the result revealed cyanide bonding at wavenumber of 2254 cm^{-1}.
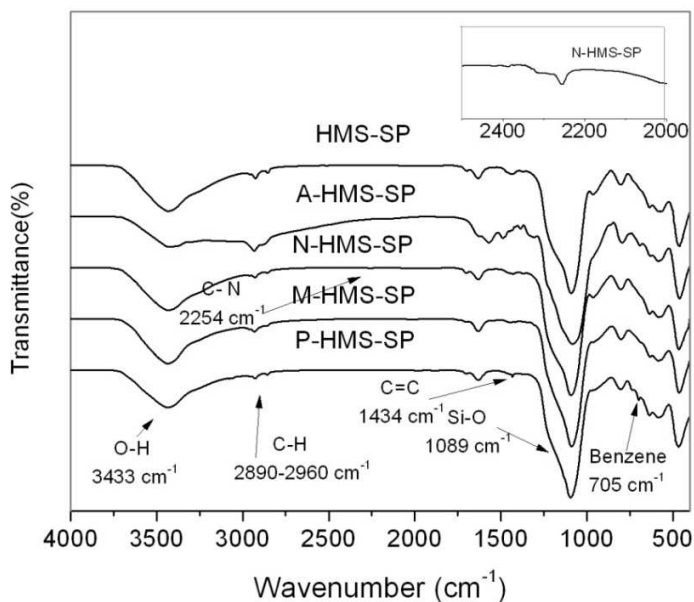
Figure 4.2 FT-IR Spectra of Synthesized Adsorbents.

4.1.4 Contact Angle

The contact angle values of hydrophobic surfaces were determined by Tensiometer. The angle value was angle between water and surface of adsorbents. The adsorbents which have high contact angle performed more hydrophobicity than adsorbent that have lower contact angle value. The measured results of contact angle was show in Table 4.2. According to Table 4.2, the order of hydrophobicity was P-HMS-SP, M-HMS-SP, N-HMS-SP, PAC and HMS-SP, respectively.

Table 4.2 Contact Angle Result of Synthesized Hydrophobic Materials

Hydrophobic material	Contact angle
M-HMS-SP	59.97±2.73
P-HMS-SP	76.62±0.02
N-HMS-SP	53.27±0.66
HMS-SP	45.06
PAC	58.343±0.08

4.1.5 SEM

The SEM images of all materials are demonstrated in Figure 4.3. The images show that all adsorbents had spherical morphology; moreover the particles have slightly different size between 100 to 300 nm.

(a)   (b)

(c)   (d)   (e)
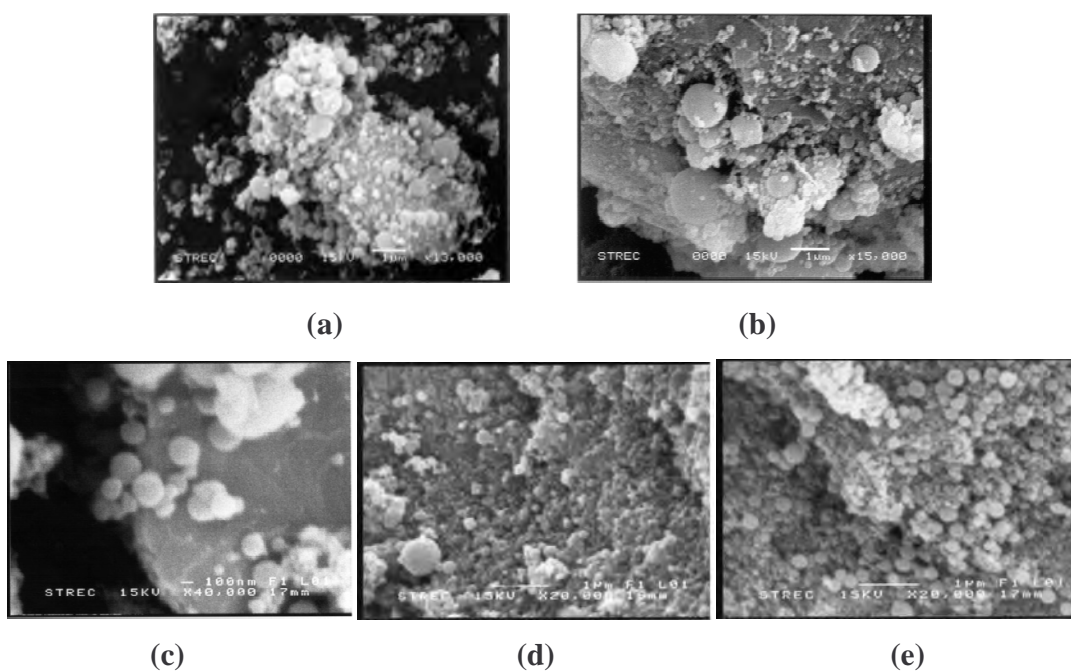
Figure 4.3 SEM Image of (a) HMS-SP, (b) A-HMS-SP, (c) M-HMS-SP, (d) P-HMS-SP and (e) N-HMS-SP.

4.1.6 Surface Charge

Surface charge of all adsorbents was measured by Zeta potential analyzer. The zeta potential profiles of HMS-SP, M-HMS-SP, A-HMS-SP, N-HMS-SP and P-HMS-SP versus pH are shown in Figure 4.4. The zero point of charge (pH_{zpc}), the balancing point between negative charges and positive charges of surface functional groups, was defined as the zero point of charge (pH_{zpc}). The pH values are summarized in Table 4.3 for all synthesized adsorbents.

According to Table 4.3, nitrile and silanol functional groups display negative charge at all pH in this study. Moreover, phenyl and mercapto functional groups perform negative charge at pH 7 and pH 9 but positive charge at pH5. The charge of amino functional group tends to be positive at pH 5 and pH 7 but has negative charge at pH 9. Surface functional groups are protonated and the positive charges are increasing at pH below pH_{zpc}. On the other hand, protons of surface functional groups are lost and the charge will perform strongly negative at pH above pH_{zpc}. The reaction of all surface functional groups will be summarized in Table 4.4.
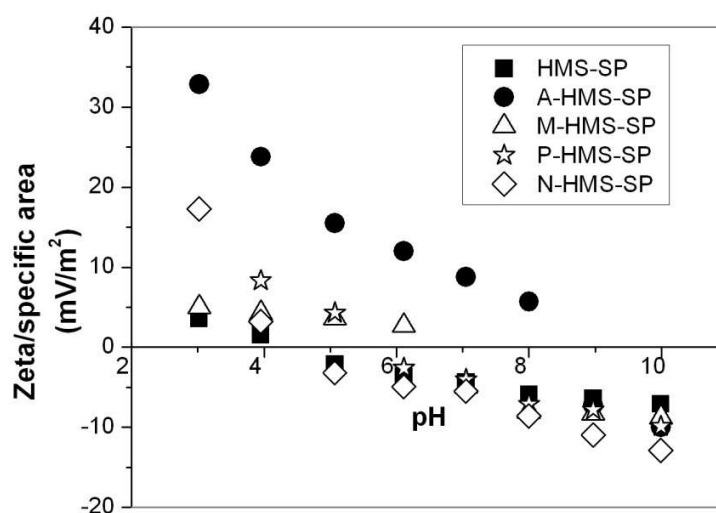
Figure 4.4 Surface Charge of Synthesized Adsorbents.

Table 4.3 pH_{zpc} of Adsorbents Used in This Study

Adsorbents	pH_{zpc}
A-HMS-SP	8.8
M-HMS-SP	6.2
HMS-SP	4.4
P-HMS-SP	5.6
N-HMS-SP	4.5

Table 4.4 Effect of pH on Surface Functional Groups (Punyapalakul, 2009)

Adsorbents	pH < pH$_{zpc}$	pH > pH$_{zpc}$
HMS-SP	$\equiv$ Si-OH + H$^+$ $\rightarrow$ $\equiv$ Si-OH$_2^+$	$\equiv$ Si-OH + OH$^-$ $\rightarrow$ $\equiv$ Si-O$^-$ + H$_2$O
A-HMS-SP	$\equiv$ Si-R-NH$_2$ + H$^+$ $\rightarrow$ $\equiv$ Si-R-NH$_3^+$	$\equiv$ Si-R-NH$_2$ + OH$^-$ $\rightarrow$ $\equiv$ Si-R-NH$_2$OH
M-HMS-SP	$\equiv$ Si-R-SH + H$^+$ $\rightarrow$ $\equiv$ Si-R-SH$_2^+$	$\equiv$ Si-R-SH + OH$^-$ $\rightarrow$ $\equiv$ Si-R-S$^-$ + H$_2$O

4.2 Adsorption Kinetic

The adsorption kinetic of NAX was conducted at pH 7$\pm$0.2 controlled by phosphate buffer at ionic strength 0.01 M, T= 25°C. The adsorptions kinetic of NAX on all adsorbents are showed in Figure 4.5. According to Figure 4.5, NAX concentrations were rapidly decreased and approached to equilibrium concentration within 1 hour for A-HMS-SP, HMS-SP and N-HMS-SP, while 9 hours for M-HMS-SP, P-HMS-SP and PAC. Obtained kinetic data were fitted by pseudo-first-order and pseudo-second-order model and displayed in Table 4.5. All kinetic experiments are matched with pseudo-second-order and rate of adsorption followed in order of affinity adsorption except P-HMS; PAC, M-HMS-SP, P-HMS-SP, N-HMS-SP, HMS-SP and A-HMS-SP, respectively. The adsorption mechanisms of all materials were investigated by intrapraticle diffusion model. This model was studied by plotting between q_t and $t^{1/2}$. For adsorption mechanism, Figure 4.6 exhibits intraparticle diffusion model. The figures are indicated that first and second step of all adsorbents were film diffusion step and intraparticle step. Film diffusion step has higher slope than intraparticle diffusion step, so the adsorption mechanism depend on the intraparticle diffusion due to their lower rate. The intraparticle diffusion is the rate limiting step of all adsirbents. For all adsorbents, the straight lines of intraparticle diffusion step pass through the origin; adsorptions of NAX were controlled by intraparticle diffusion step, except M-HMS-SP and PAC. Figure 4.6 (f) demonstrated that second step and third step are intraparticle diffusion of micro pore and meso pore of PAC. In case of PAC and M-HMS-SP, it indicated that intraparticle diffusion step is not only the rate limit step of adsorption mechanism due to their interception of straight line.
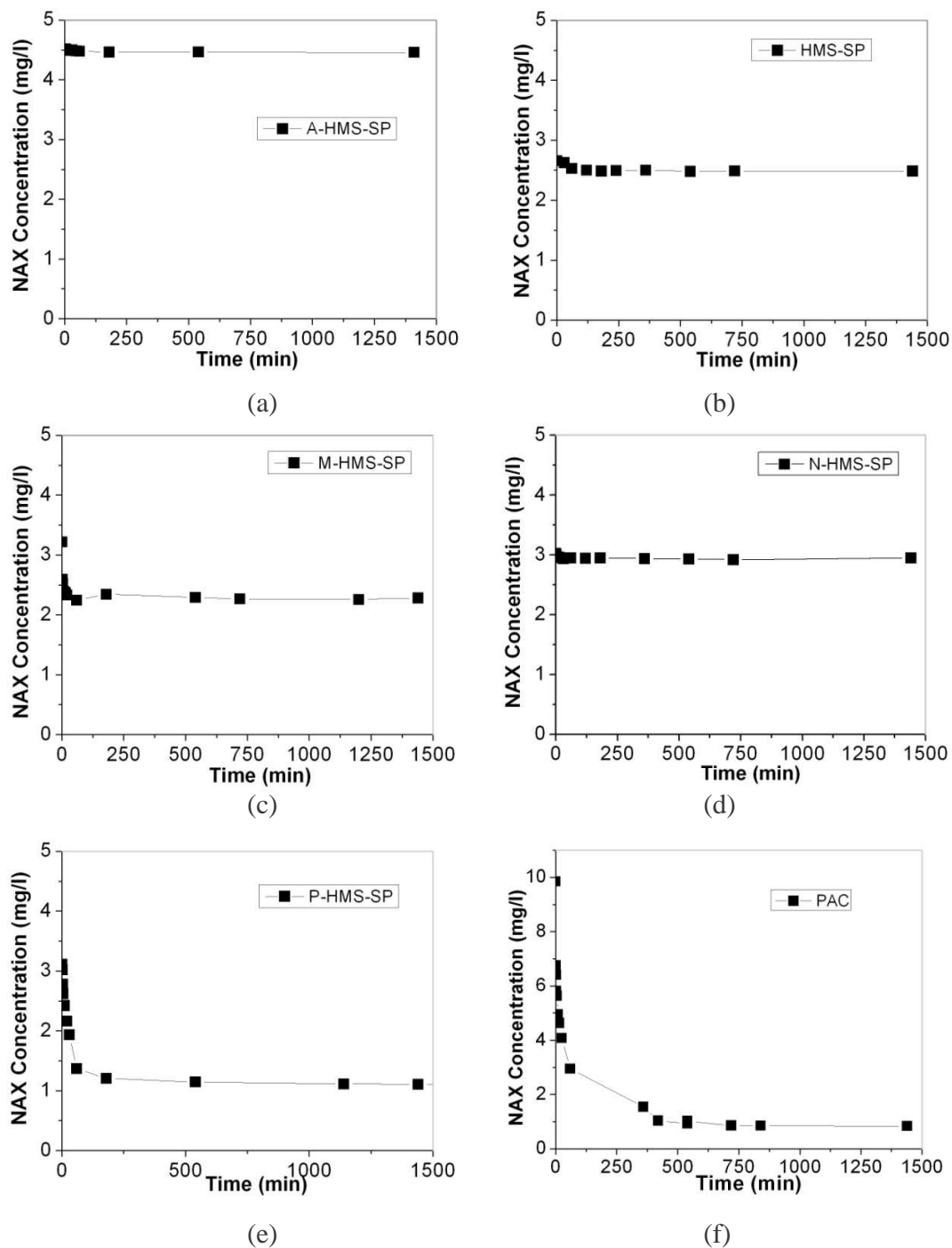
Figure 4.5 Adsorption Kinetic Results of NAX on All Adsorbents; (a) A-HMS-SP, (b) HMS-SP, (c) M-HMS-SP, (d)N-HMS-SP, (e) P-HMS-SP and (f)PAC at 25 ± 2 °C, pH 7 ± 2, and 0.01 M Ionic Strength.

Table 4.5 Experiment Data of Adsorption Kinetic

Adsorbents	Pseudo-first order		Pseudo-second order				
	R^2	k_1 (1/min)	R^2	k_2 (g/mg·min)	Calculated q_e (mg/g)	Experimental q_e (mg/g)	h^* (mg/g·min)
A-HMS-SP	0.8655	-0.002	0.9981	0.7773	0.0441	0.0414	0.0015
M-HMS-SP	0.5799	-0.001	0.9997	0.6145	0.7094	0.7198	0.3092
HMS-SP	0.5913	-0.002	0.9912	0.1620	0.1357	0.1299	0.0030
P-HMS-SP	0.8122	-0.003	0.9999	0.0382	1.5244	1.5000	0.0888
N-HMS-SP	0.6394	-0.017	0.9974	0.5118	0.1374	0.1326	0.0097
PAC	0.9802	-0.003	0.9997	0.0007	135.1351	135.1112	13.2100

h^* = initial adsorption rate (mg/g h) calculated from $h = k_2 q_e^2$.
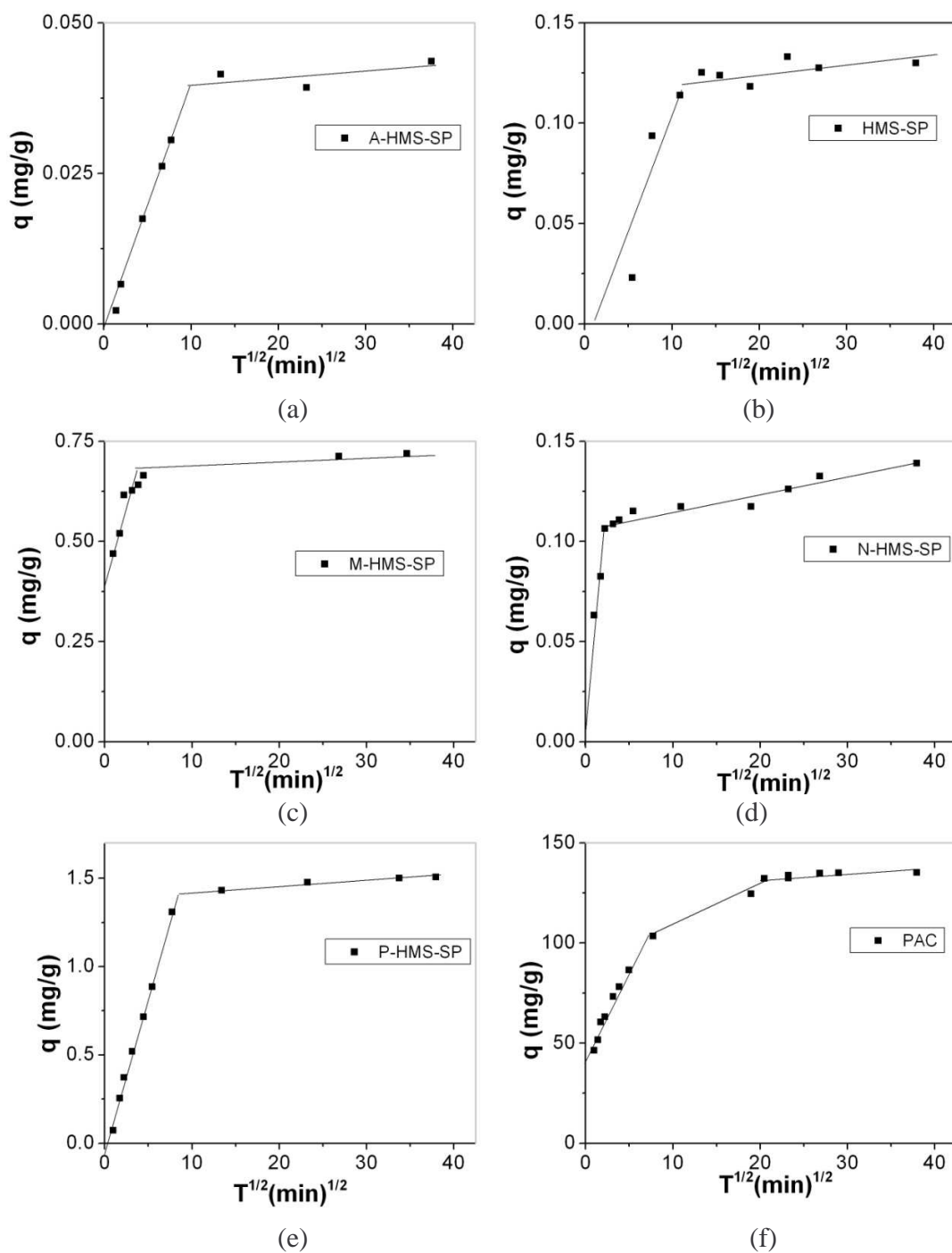
Figure 4.6 Intraparticle Diffusion of Adsorbents; (a) A-HMS-SP, (b) HMS-SP, (c) M-HMS-SP, (d)N-HMS-SP, (e) P-HMS-SP and (f)PAC.

4.3 Adsorption Isotherm

4.3.1 Effect of Surface Functional Groups at pH 7± 0.2

NAX adsorption isotherms of six adsorbents at pH 7 were shown in Figure 4.7, it is revealed that phenyl had the highest adsorption capacity following with 3-mercaptopropyl, nitrile, silanol groups on pristine HMS-SP and 3-aminopropyltriethoxy, respectively. However, adsorption capacity of PAC still is higher than all synthesized adsorbents. Van der Waals interaction caused by hydrophobicity was suggested to play the most important role for NAX adsorption on hydrophobic adsorbents surface. The affinity adsorptions on hydrophobic adsorbents followed in order of hydrophobicity material; P-HMS-SP, M-HMS-SP and N-HMS-SP. For Figure 4.8, occurrence of hydrogen bonding of HMS-SP was proved by FTIR. Comparing free O-H stretching between silanol group on pristine and NAX adsorbed HMS in hexane. It was found that after NAX adsorption in hexane free O-H stretching of HMS did not shift from virgin HMS. However, the shape of HMS that adsorbed NAX in hexane was slightly changed from the shape of virgin HMS at 3200 cm^{-1}. Moreover, 2930 cm^{-1} and 1444 cm^{-1} demonstrated the existence of aromatic ring of NAX. Adsorption of NAX by silanol groups on HMS might involve in hydrogen bonding interaction. However, a bit adsorption capacity of NAX on HMS-SP can be detected. It could be suggested that effect of water in NAX solution might be interrupt to NAX adsorption by hydrogen bonding on HMS-SP due to carboxylic of NAX competed with O-H of water. At pH 7, all synthesized materials performed repulsive interaction except A-HMS-SP that performed attractive interaction due to pH$_{zpc}$ >7, but the attractive interaction of amino group did not enhance adsorption capacity comparing hydrophobic force. It might cause that A-HMS-SP had lower possibility to adsorb NAX than hydrophobic adsorbents due to accessibility to pollutant. The effect of pore size diameter can be neglect for all adsorbents due to molecular size of NAX.
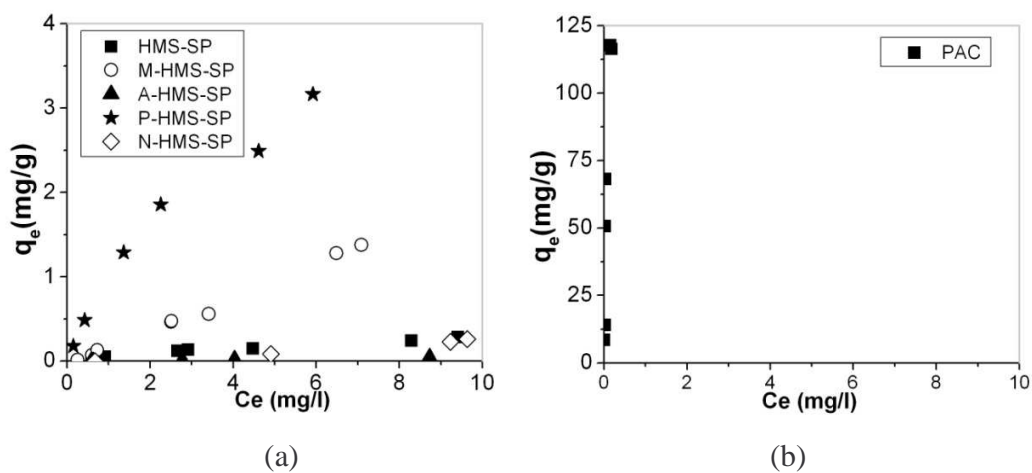
Figure 4.7 Adsorption Capacities of NAX on Synthesized Adsorbents (a) and PAC (b) at 25$\pm$2 °C, pH 7$\pm$0.2, and 0.01 M Ionic Strength.
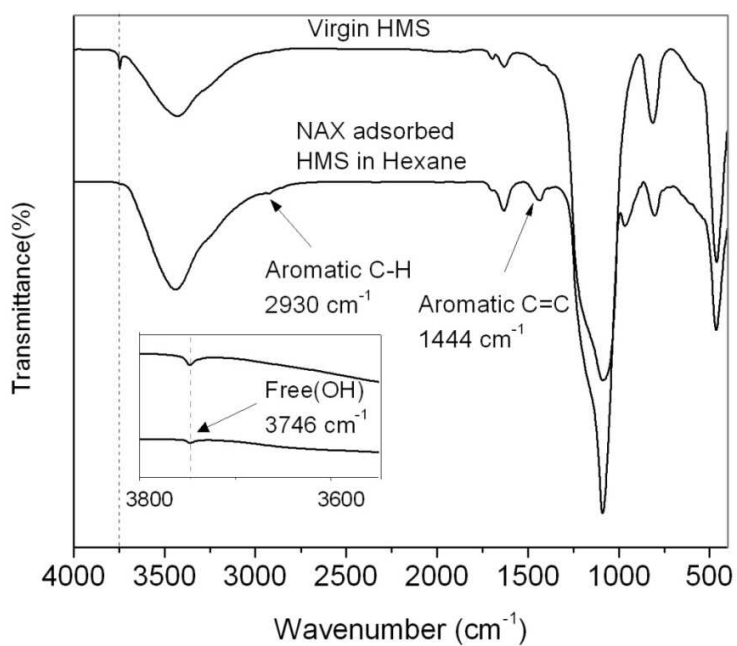
Figure 4.8 FT-IR of Virgin HMS and NAX Adsorbed HMS in Hexane.

To evaluate effect of surface functional groups on NAX adsorption capacities, adsorption capacity per square meter were compared to eliminate effect of surface area of adsorbents. As shown in Figure 4.9, the order of adsorption affinity did not change

significantly; PAC, P-HMS-SP, M-HMS-SP, N-HMS-SP, HMS-SP and A-HMS-SP, respectively. The adsorption capacity per square meter of HMS-SP was not significantly different comparing with A-HMS-SP, which might be caused by electrostatic force.

(a)   (b)
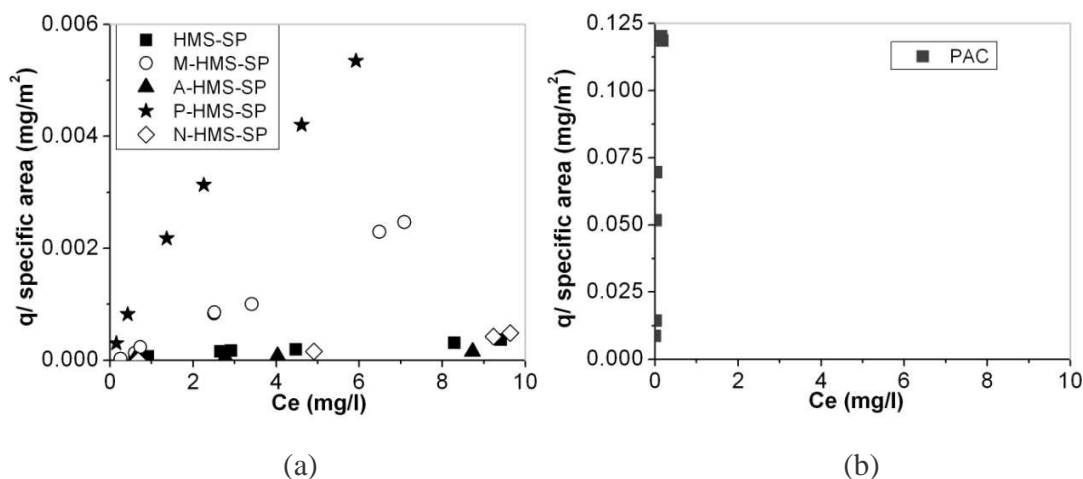
Figure 4.9 Adsorption Capacities Per Specific Surface Area of NAX on Synthesized
Adsorbents (a) and PAC (b) at 25 ± 2 °C, pH 7 ± 0.2, and 0.01 M Ionic Strength.

4.3.2 Effect of pH

Effect of pH on adsorption capacities of adsorbents were determined by varying pH of solution between 5, 7, and 9 at IS 0.01 M controlled by phosphate buffer. Table 4.6 shows relationship between surface charge of adsorbents and NAX at pH 5, 7 and 9. NAX adsorption isotherms at pH 5-9 were plotted and compared in Figure 4.10. It was found that adsorption capacities at pH 5 and 9 of silanol and amino grafted adsorbent (A-HMS-SP and HMS-SP, respectively) did not change significantly comparing with adsorption capacity at pH7. However, effect of pH influences on adsorption of NAX on PAC, P-HMS-SP, M-HMS-SP and N-HMS-SP. For PAC, the capacity was enhanced by reducing pH due to expanding attractive force of electrostatic interaction. Adsorption capacity of N-HMS-SP at pH 5 was strongly changed comparing with pH 7 and pH 9, it might be that pH 5 was closely to pH_{zpc} of N-HMS-SP and then possibility of adsorption might be increased by increasing of attractive interaction between adsorbent and

pollutant. In case of M-HMS-SP and P-HMS-SP, adsorption capacities were increased with attractive interaction at pH 5 and decreased with repulsive interaction at pH 9. It could be indicated that combination of electrostatic interaction and hydrophobic force might affect on adsorption capacity of M-HMS-SP and P-HMS-SP.

Table 4.6 Charges Relationship between Adsorbents and NAX.

| Adsorbents/ Pollutant	pHzpc/ pKa	pH5		pH7		pH9	
		Charge	Interaction	Charge	Interaction	Charge	Interaction
NAX	4.15	-		-		-	
HMS-SP	4.4	-	Repulsive	-	Repulsive	-	Repulsive
A-HMS-SP	8.8	+	Attractive	+	Attractive	-	Repulsive
M-HMS-SP	6.2	+	Attractive	-	Repulsive	-	Repulsive
P-HMS-SP	5.6	+	Attractive	-	Repulsive	-	Repulsive
N-HMS-SP	4.5	-	Repulsive	-	Repulsive	-	Repulsive
PAC	9.8	+	Attractive	+	Attractive	+	Attractive

(a)   (b)
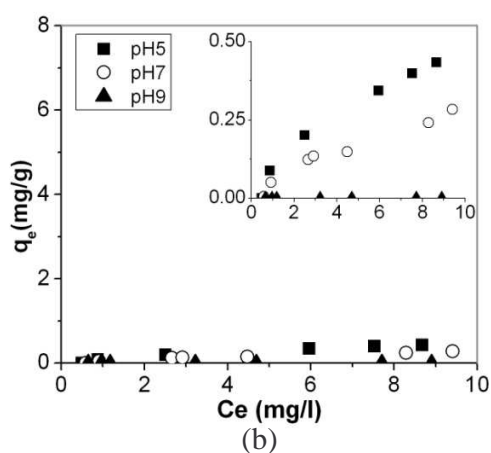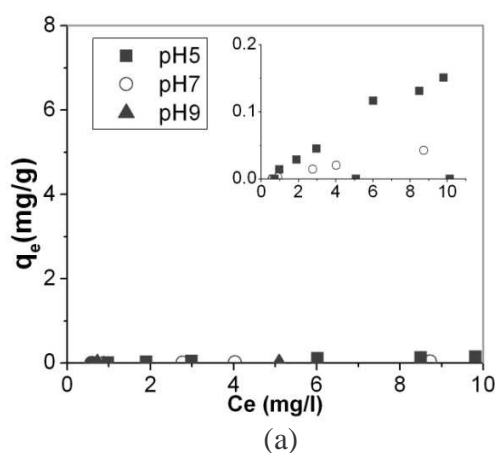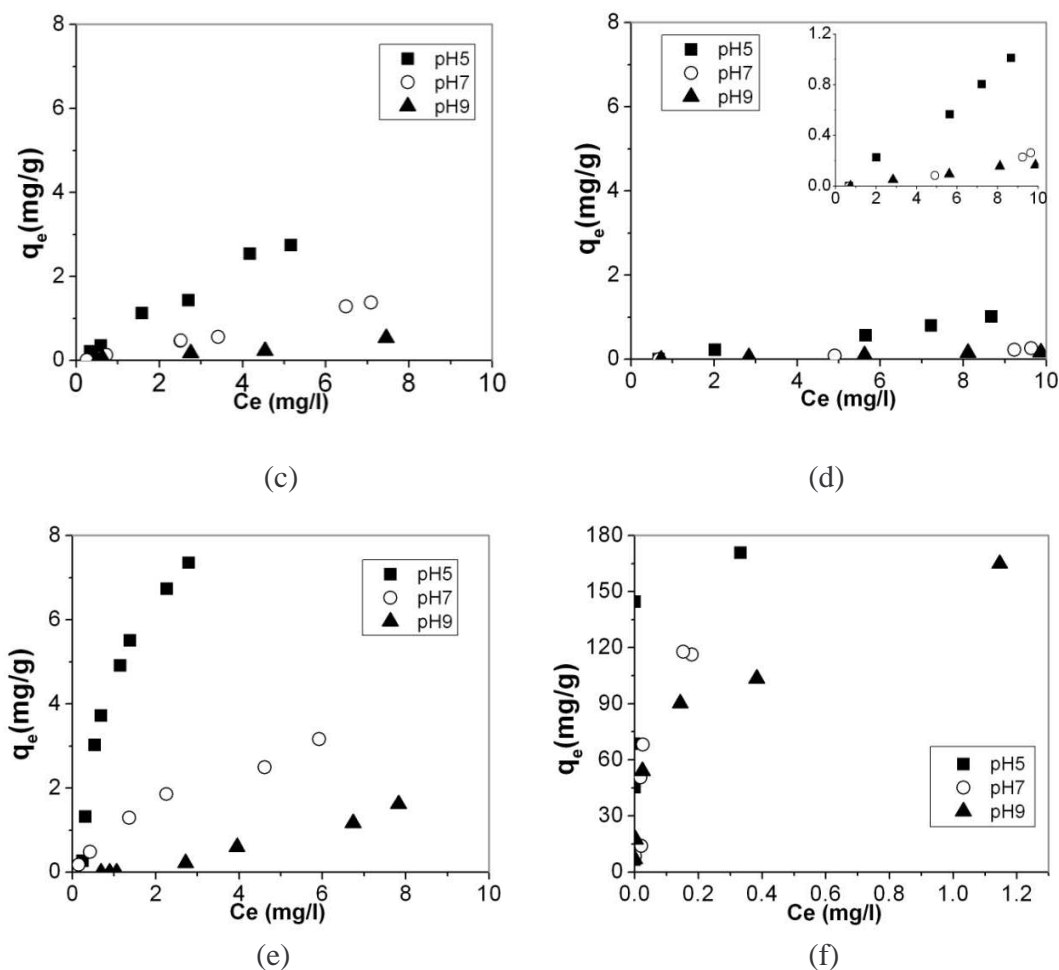
Figure 4.10 Adsorption Capacities of NAX on Adsorbents; (a) A-HMS-SP, (b) HMS-SP, (c) M-HMS-SP, (d) N-HMS-SP, (e) P-HMS-SP and (f) PAC at 25±2 °C and 0.01 M Ionic Strength.

Adsorption isotherms of all adsorbents at pH 5, 7, and 9 were fitted with linear Freundlich isotherm model and Langmuir model that shown in Table 4.7 and Table 4.8. It was found that experimental data can be matched with linear, Freundlich model and Langmuir model and the correlation coefficients were not significant different. According Table 4.7, the results of adsorption isotherm were mostly suitable with Freundlish model.

Table 4.7 Experiment Data of Linear and Freundlish Isotherm

Adsorbents	Linear		Freundlish		
	a (slope)	R^2	K_F	n	R^2
HMS-SP					
pH5	0.0491	0.9592	0.0882	1.3381	0.9713
pH7	0.0271	0.9393	0.0556	1.3949	0.9606
pH9	N/A	N/A	N/A	N/A	N/A
A-HMS-SP					
pH5	0.0164	0.9753	0.0171	1.0312	0.9699
pH7	0.0053	0.9919	0.0043	0.9300	0.9794
pH9	N/A	N/A	N/A	N/A	N/A
M-HMS-SP					
pH5	0.5514	0.9828	0.6413	1.0978	0.9819
pH7	0.1980	0.9929	0.1538	0.8906	0.9944
pH9	0.0691	0.9545	0.0404	0.7866	0.9556
P-HMS-SP					
pH5	2.4926	0.8668	4.0418	1.5545	0.9111
pH7	0.4819	0.9529	1.0064	1.5752	0.9838
pH9	0.2213	0.9793	0.0487	0.5904	0.9897
N-HMS-SP					
pH5	0.1205	0.9915	0.0742	0.8306	0.9886
pH7	0.0465	0.7567	0.00002	0.2416	0.9711
pH9	0.0185	0.9869	0.0157	0.9568	0.9791
PAC					
pH5	N/A	N/A	N/A	N/A	N/A
pH7	552.48	0.8203	273.8735	2.1136	0.8382
pH9	119.2	0.8114	154.5021	3.2124	0.9804

Table 4.8 Experiment Data of Langmuir Isotherm

Adsorbents	Langmuir		
	Q_m	B	R^2
HMS-SP			
pH5	0.9140	0.1030	0.9816
pH7	0.5893	0.0915	0.9664
pH9	N/A	N/A	N/A
A-HMS-SP			
pH5	1.1123	0.0164	0.9726
pH7	N/A	N/A	N/A
pH9	N/A	N/A	N/A
M-HMS-SP			
pH5	15.8754	0.0421	0.9833
pH7	N/A	N/A	N/A
pH9	N/A	N/A	N/A
P-HMS-SP			
pH5	12.6919	0.5181	0.9512
pH7	5.1530	0.2390	0.9870
pH9	N/A	N/A	N/A
N-HMS-SP			
pH5	N/A	N/A	N/A
pH7	N/A	N/A	N/A
pH9	N/A	N/A	N/A
PAC			
pH5	N/A	N/A	N/A
pH7	153.7700	19.3182	0.8439
pH9	156.4944	0.1130	0.8826

4.4 Separation

The experiments were conducted using column which has an internal diameter of 0.8 cm and height of 15 cm. The magnetic stainless filter was induced by approximately 0.2

T of magnets. P-HMS-SP was selected to study separation efficiency of HGMS filter due to the highest NAX adsorption capacity.

4.1.1 Physical Characteristic of Stainless Filter

The vernier was used to determine width and length of stainless filter. The surface area per gram and volume per gram were calculated in eq. 4.1 and 4.2. The data were summarized in Table 4.9.

$$S = \frac{(2W \cdot D + 2W \cdot H + 2H \cdot D)}{weigth} \tag{4.1}$$

$$\rho = \frac{(W \cdot D \cdot H)}{weigth} \tag{4.2}$$

Where S is surface area (cm^2/g), W is width of stainless filter (mm), D is length of stainless filter (mm), H is height (mm) and ρ is density of stainless filter (g/cm^3).

Table 4.9 Parameters Characteristic of Stainless Filter

Parameters	Values
Width	0.46mm
Height	0.04mm
Surface area	98.3935cm^2/g
Density	5.5443 g/cm^3

4.1.2 Effect of Flow Rate, Surface area and Depth Length of Stainless Filter

This experiment was designed breakthrough concentration of particle at 10% removal. Figure 4.11 (a) show breakthrough curve at different depth length of stainless filter at constant flow rate (0.95 cm/min), concentration particle (0.5 g/L) and surface area of stainless filter (37.23 cm^2). It can be seen that the breakthrough time at breakthrough concentration was increased when extending bed depth due to higher surface area and contact time. For effect of flow rate, it was indicated that slower flow

rate performed longer breakthrough time at 10% breakthrough by increasing contact time as shown in Figure 4.10 (b) under fixed bed depth (5 cm), concentration particle (0.5 g/L) and surface area(37.23 cm^2). Surface area of stainless filter at 37.23 cm^2 and 49.66 cm^2 were not significantly influence on breakthrough time and filtrate volume. Decrease of surface area to 19.32 cm^2 caused the reduce of service volume due to lower contact surface area, as shown in Figure 4.11 (c).

(a)

(b)

(c)
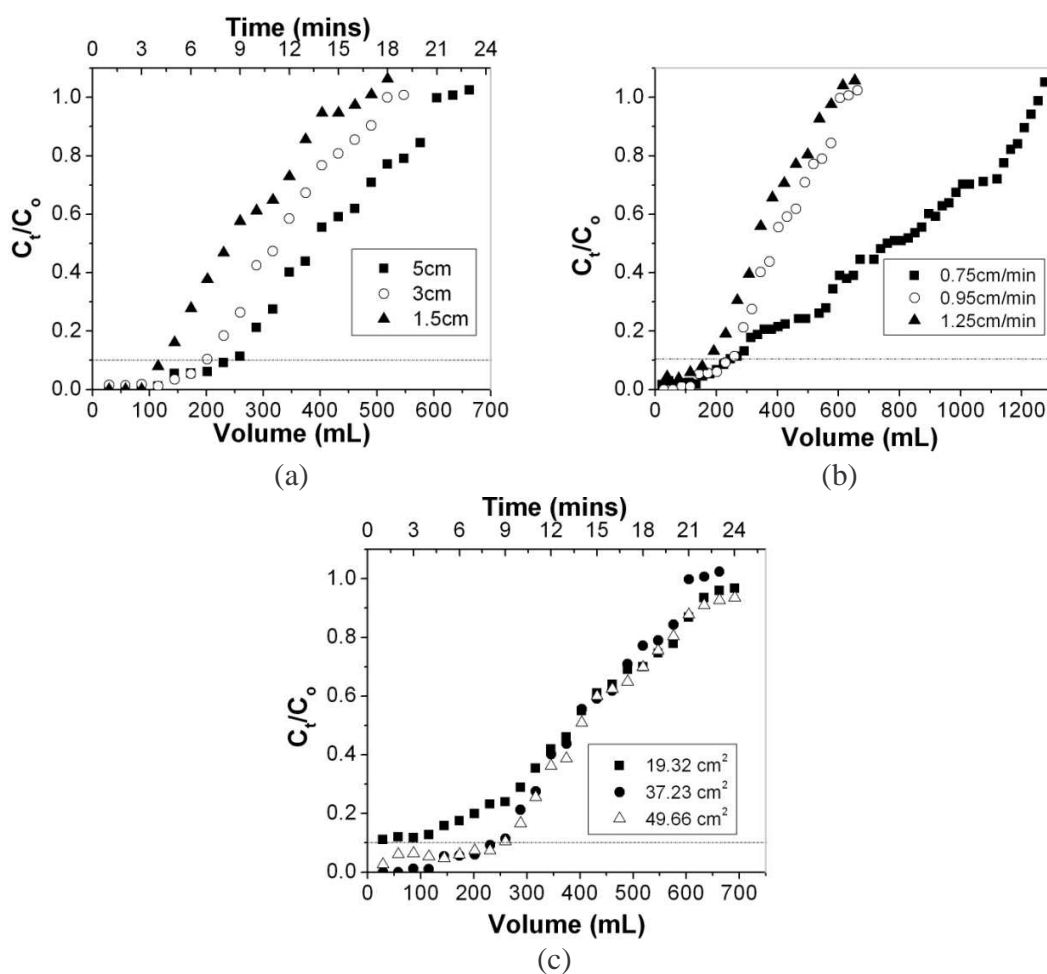
Figure 4.11 Effect of (a) Bed Depth Stainless Filter, (b) Flow Rate and (c) Surface Area of Stainless Filter on Breakthrough Curve.

According to Table 4.10, efficiency of stainless filter in different condition was analyzed in equation 4.3. This Table demonstrated that the best condition is 1.5 cm of bed depth, 0.95 cm/min of flow rate and 37.23 cm^2 of surface area due to slightly different in flow rate between 0.95 and 0.75 cm/min.

$$Q = \frac{t \times F}{S} \qquad\qquad (4.3)$$

Where Q is breakthrough capacity (cm^3/cm^2), t is time at breakthrough at 10% (min), F is flow rate (cm^3/min) and S is surface area (cm^2).

Table 4.10 Experiment Data and Breakthrough Capacity of Various Depth, Flow Rate and Surface Area

Parameter	Breakthrough Time (min)	Filtrated Volume at Breakthrough (cm^3)	Breakthrough Capacity (cm^3/cm^2)
Varying Depth			
1.5 cm	4.58	132.0	11.8198
3 cm	6.92	199.2	8.9186
5 cm	8.36	240.9	6.4714
Varying Flow			
0.75 cm/min	10.78	241.5	6.4883
0.95 cm/min	8.36	240.9	6.4714
1.25 cm/min	4.02	160.7	4.3170
Varying Surface area			
49.66 cm^2	8.50	244.9	4.9323
37.23 cm^2	8.36	240.9	6.4714
19.32 cm^2	-	-	-

4.1.3   Effect of Particle Concentration and Adsorbed NAX

The effect of particle concentration was investigated by vary concentrations from 0.3 to 1 g/L as demonstrated in Figure 4.12 (a). It can be seen that increasing particle concentration had lower breakthrough times; 18.2, 8.64 and 6.33 min for 0.3, 0.5 and 1g/L, respectively. It might suggest that low density of particles were captured easier than at high density because low density flux had more remained space to catch the particle than high density flux.

In order to study effect of NAX on separation efficiency of HGMS filtration, the best conditions obtained from previous experiment were applied with particles that adsorbed at initial concentration 5 mg/L of NAX. Adsorption capacity of NAX on P-HMS-SP in HGMS filter (2.8 mg/g) did not significantly different from capacity in batch experiment (2.5 mg/g). Comparison between with and without NAX shown that breakthrough time of adsorbed NAX particle (4.09 min) was slightly change from non-adsorbed NAX particle (4.58 min) (Figure 4.12 (b)). It can indicate that adsorbed NAX on P-HMS-SP did not affect on separation efficiency of HGMS filter. Moreover, effect of magnetic flux density influenced on filtration due to filtration under above conditions was not active without magnetic flux density.

(a)   (b)
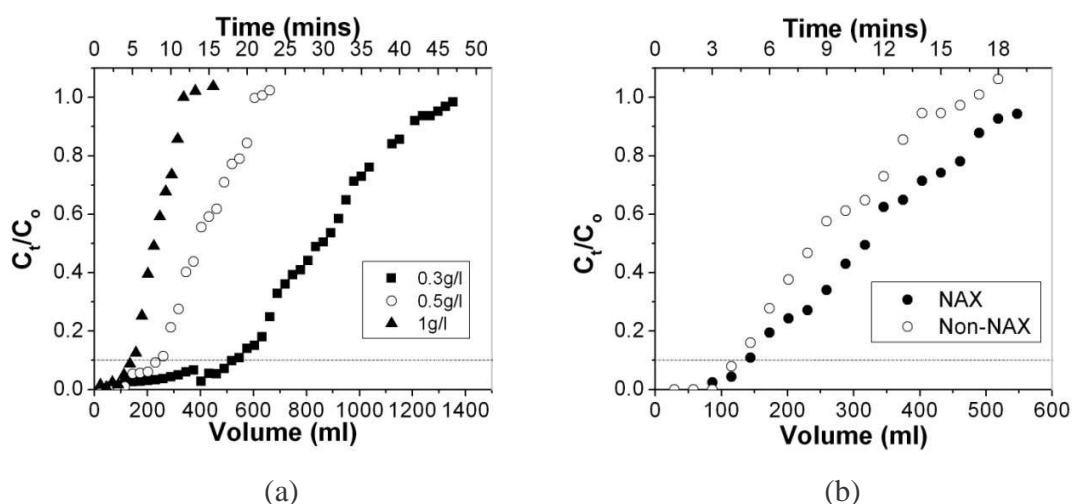
Figure 4.12 Effect of (a) Particle Concentration and (B) Adsorbed NAX.

4.1.4   Apply of BDST Model

The experimental data were plot in linear regression between breakthrough time and bed depth from bed depth service time (BDST) equation which is commonly model to apply in column as shown in Figure 4.13. The parameter values are obtained from slope and intercept of this graph and shown as Table 4.11. According to Figure 4.13 and Table 4.11, it demonstrated that BDST model was successfully used to apply HGMS filter due to high correlation coefficient. However, HGMS filter did not have critical depth because magnetic force from magnet outside the column might help to separate magnetic particles from synthesized wastewater.

$$t = \frac{N_0}{C_0 V}\left[D - \frac{V}{KN_0}\ln\left(\frac{C_0}{C_B} - 1\right)\right] \qquad (4.1.1)$$

$$a = \frac{N_0}{C_0 V} \qquad (4.1.2)$$

$$b = \frac{1}{C_0 K}\ln\left(\frac{C_0}{C_B} - 1\right) \qquad (4.1.3)$$

Where t is time at breakthrough (hr.), V is linear flow rate (cm/hr), D is bed depth of adsorbent (cm), K is rate constant (L/(mg·hr)), N_0 is adsorption capacity (g/L), C_0 is influent solute concentration (g/L) and C_B is solute concentration at breakthrough (g/L).
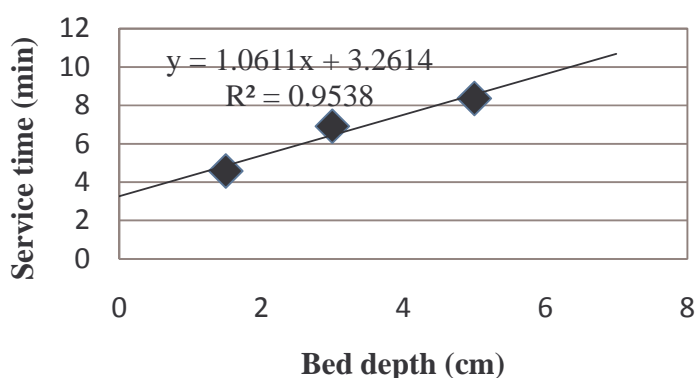
Figure 4.13 The BDST Model at 0.5g/L of Particle Concentration, Flow Rate: 0.95cm/min.

Table 4.11 Calculated data from BDST model

C_0 (g/L)	K (L/(mg·hr))	N_0 (g/L)	R^2
0.5	-1.347	30.24	0.9538

Predicted breakthrough time was calculated by adjusted slope and intercept of linear equation. The slope and intercept of this equation by changing flow rate and particle concentration were adjusted as equation 4.2 for flow rate and equation 4.3 for particle concentration. Table 4.12 showed predicted and experimental time at breakthrough in different particle concentration and flow rate under constant bed depth of 5 cm and 37.23 cm^2 surface area of stainless. According to Table 4.12, the predicted times of changed particle concentration and flow rate did not match with experimental times. It was found that adjusted equation to predicted breakthrough time was not achieved. It might be caused by attachment mechanism of P-HMS-SP on stainless filter surface do not relate to particle concentration. Hence, relationship of breakthrough time and initial concentration of P-HMS-SP could not be detected. However, BDST model could be applied to predict breakthrough time under fixed influent concentration of the particles.

$$t = a'x + b \qquad\qquad (4.2.1)$$

$$a' = \frac{V \cdot a}{V'} \qquad\qquad (4.2.2)$$

$$t = a'x + b' \qquad\qquad (4.3.1)$$

$$a' = \frac{C_0 \cdot a}{C_1} \qquad\qquad (4.3.2)$$

$$b' = b \left(\frac{C_0}{C_1}\right) \frac{\ln[(C_1/C_F)-1]}{\ln[(C_0/C_B)-1]} \qquad\qquad (4.3.3)$$

Where t is time at breakthrough (hr), x is bed depth (cm), a is old slope, a' is new slope, b is ordinate intercept. b and b' are old and new intercept, C_0 and C_1 are old and new influent solute concentration (g/L) and C_B and C_F are old and new effluent solute concentration (g/L).

Table 4.12 Comparison of the Theoretical Breakthrough Times with Experimental Breakthrough Time

Parameter	Predicted breakthrough time (min)	Experimental breakthrough time (min)
Particle concentration		
0.3 g/L	7.20	18.20
1 g/L	2.16	6.33
Flow rate		
0.75 cm/min	10.08	10.78
1.25 cm/min	7.24	4.08

CHAPTER V
CONCLUSION AND RECOMMENDATIONS

5.1   Conclusion

The main objectives of this study are to investigate adsorption capacities of naproxen (NAX) on functionalized superparamagnetic mesoporous silicates (SP-MS) comparing with powdered activated carbon (PAC) and to evaluate possibility to separate functionalized SP-MSs by high gradient magnetic separation filter (HGMS filter).

The superparamagnetic hexagonal mesoporous silicates were synthesized by coating synthesized magnetite with tetraethylorthosilicate (TEOS) and dodecylamine. There are five functional groups for synthesis adsorbents by co-condensation method including; mercapto, amino, nitrile, phenyl and silanol on pristine HMS-SP.

Physico-chemical characteristic were analyzed by FTIR, N_2 adsorption, contact angle, Zeta potential and SEM. The reports from all measurements were indicated that all synthesized adsorbents had size diameter between 100-300nm and pore size diameter of it were 5nm to 12 nm. The pHzpc values of all adsorbents were used to describe effect of pH on adsorption mechanism.

Adsorption kinetic was conducted at pH 7 ± 0.2 controlled by phosphate buffer at ionic strength 0.01 M, T= 25°C. The data were fit with pseudo-second-order model. It was found that the equilibrium times of all adsorbents are 1 hour for A-HMS-SP, HMS-SP and N-HMS-SP, while 9 hours for M-HMS-SP, P-HMS-SP and PAC. To investigate adsorption mechanism by intraparticle diffusion model, the result showed that adsorptions of NAX were controlled by intraparticle diffusion step, except M-HMS-SP and PAC.

To study adsorption isotherm, the experiments were run at 25 ± 2 °C and 0.01 M ionic strength. PAC had the highest adsorption capacity following with phenyl-, 3-mercaptopropyl-, nitrile, silanol groups on pristine HMS-SP and 3-aminopropyltriethoxy-respectively. Hydrophobicity of phenyl group on silicate porous surface influences on adsorption mechanism of NAX. The electrostatic force effects on adsorption capacity

except amino and silanol grafted adsorbent. It could be indicated that combination of electrostatic interaction and hydrophobic force might affect on adsorption capacity of M-HMS-SP and P-HMS-SP.

To investigate separation magnetic particle by HGMS filter, the breakthrough time was increasing by extending bed depth of stainless filter and decreasing flow rate. However, higher and lower surface area of stainless filter did not affect to breakthrough curve but it can be failed when surface area was not enough as seen at 19.32 cm^2. To determine effect of particle concentration, low density of particles were captured easier than high density because low density had more remained space to catch the particle than high density. Comparison of breakthrough capacity, it indicated that the best condition is 1.5 cm of bed depth, 0.95 cm/min of flow rate and 37.23 cm^2 of surface area of stainless steel. Breakthrough curve of adsorbed NAX solution in the best condition did not significantly change from non-adsorbed NAX solution. Moreover, application of BDST model can be matched with HGMS filter, due to high correlation coefficient. Nevertheless, BDST model cannot apply with changing flow rate and particle concentration.

5.2   Recommendations

5.2.1   Adsorption mechanism of NAX on functionalized hexagonal mesoporous silicates at low concentration should be investigated.

5.2.2   Effect of intensity of magnetic field on HGMS filter should be evaluated.

5.2.3   Regeneration of adsorbents should be investigated.

REFERENCES

Agency U.S.Environmental Protection. BCES: Module 3 - Characteristics of Particles [Online]. 2010. Available from: http://www.epa.gov/eogapti1/bces/module3/collect/collect.htm,

Akpa O. M. ,and Unuabonah E. I. Small-Sample Corrected Akaike Information Criterion: An appropriate statistical tool for ranking of adsorption isotherm models. Desalination 272 (2011): 20-26.

Baik S. K., Ha D. W., Ko R. K. ,and Kwon J. M. Magnetic field and gradient analysis around matrix for HGMS. Physica C: Superconductivity 470 (2010): 1831-1836.

Boyd G. R., Palmeri J. M., Zhang S. ,and Grimm D. A. Pharmaceuticals and personal care products (PPCPs) and endocrine disrupting chemicals (EDCs) in stormwater canals and Bayou St. John in New Orleans, Louisiana, USA. Science of The Total Environment 333 (2004): 137-148.

Boyd G.R.l, Zhang S. ,and Grimm D. A. Naproxen removal from water by chlorination and biofilm processes. Water Research 39 (2005): 668-676.

Bui T.X., and Choi, H. Adsorptive removal of selected pharmaceuticals by mesoporous silica SBA-15. Journal of Hazardous Materials 168 (2009): 602-608.

Burleigh M. C., Markowitz M. A., Spector M. S. ,and Gaber B. P. Direct Synthesis of Periodic Mesoporous Organosilicas: Functional Incorporation by Co-condensation with Organosilanes. The Journal of Physical Chemistry B 105 (2001): 9935-9942.

Carballa M., Omil F., Lema J. M., Llompart M., García-Jares C., Rodríguez I., Gómez M. ,and Ternes T. Behavior of pharmaceuticals, cosmetics and hormones in a sewage treatment plant. Water Research 38 (2004): 2918-2926.

Cleuvers M. Mixture toxicity of the anti-inflammatory drugs diclofenac, ibuprofen, naproxen, and acetylsalicylic acid. Ecotoxicology and Environmental Safety 59 (2004): 309-315.

Cuerda-Correa E. M., Domínguez-Vargas J. R., Olivares-Marín F. J. ,and de Heredia J. B. On the use of carbon blacks as potential low-cost adsorbents for the removal of non-steroidal anti-inflammatory drugs from river water. Journal of Hazardous Materials 177 (2010): 1046-1053.

Dave S. R. ,and Gao X. Monodisperse magnetic nanoparticles for biodetection, imaging, and drug delivery: a versatile and evolving technology. <u>Wiley Interdisciplinary Reviews: Nanomedicine and Nanobiotechnology</u>1 (2009): 583-609.

DellaGreca M., Brigante M., Isidori M., Nardelli A., Previtera L., Rubino M. ,and Temussi F. Phototransformation and ecotoxicity of the drug Naproxen-Na. <u>Environmental Chemistry Letters</u> 1 (2003): 237-241.

Deng Y. H., Wang C.C., Hu J.H., Yang W.L. ,and Fu S.K. Investigation of formation of silica-coated magnetite nanoparticles via sol-gel approach. <u>Colloids and Surfaces A: Physicochemical and Engineering Aspects</u> 262 (2005): 87-93.

Ditsch A., Lindenmann S., Laibinis P. E., Wang D. I. C. ,and Hatton T. Alan. High-Gradient Magnetic Separation of Magnetic Nanoclusters. <u>Industrial & Engineering Chemistry Research</u> 44 (2005): 6824-6836.

Fent K., Weston A. ,and Caminada D. Ecotoxicology of human pharmaceuticals. <u>Aquatic Toxicology</u> 76 (2006): 122-159.

Fornara A. <u>Magnetic nanostructured materials for advanced bio-applications</u>. Microelectronics and Applied Physics, School of Information and Communication Technology Royal Institute of Technology, 2008.

Gagnon C., Lajeunesse A., Cejka P., Gagné F. ,and Hausler R. Degradation of Selected Acidic and Neutral Pharmaceutical Products in a Primary-Treated Wastewater by Disinfection Processes. <u>Ozone: Science & Engineering: The Journal of the International Ozone Association</u> 30 (2008): 387 - 392.

Gupta A. K. ,and Gupta M.. Synthesis and surface engineering of iron oxide nanoparticles for biomedical applications. <u>Biomaterials</u> 26 (2005): 3995-4021.

Han R., et al. Adsorption of methylene blue by phoenix tree leaf powder in a fixed-bed column: experiments and prediction of breakthrough curves. <u>Desalination</u> 245 (2009): 284-297.

Han R., Zhang J., Han P., Wang Y., Zhao Z. ,and Tang M. Study of equilibrium, kinetic and thermodynamic parameters about methylene blue adsorption onto natural zeolite. <u>Chemical Engineering Journal</u> 145 (2009): 496-504.

Hua J., An P., Winter J. ,and Gallert C. Elimination of COD, microorganisms and pharmaceuticals from sewage by trickling through sandy soil below leaking sewers. <u>Water Research</u> 37 (2003): 4395-4404.

Isidori M., Lavorgna M., Nardelli A., Parrella A., Previtera Lucio ,and Rubino Maria. Ecotoxicity of naproxen and its phototransformation products. Science of The Total Environment 348 (2005): 93-101.

Jones O. A. H., Voulvoulis N. ,and Lester J. N. Aquatic environmental assessment of the top 25 English prescription pharmaceuticals. Water Research 36 (2002): 5013-5022.

Joon-Woo K., et al. Occurrence of Pharmaceutical and Personal Care Products(PPCPs) in Surface Water from Mankyung River, South Korea. Journal of Health Science 55 (2009): 249-258.

Joss A., et al. Removal of pharmaceuticals and fragrances in biological wastewater treatment. Water Research 39 (2005): 3139-3152.

Kailas S.V. Chapter 16. Magnetic properties. I. I. o. Science. India.

Khan S. J. ,and Ongerth J. E. Modelling of pharmaceutical residues in Australian sewage by quantities of use and fugacity calculations. Chemosphere 54 (2004): 355-367.

Khetan S. K. ,and Collins T. J. Human Pharmaceuticals in the Aquatic Environment: A Challenge to Green Chemistry. Chemical Reviews 107 (2007): 2319-2364.

Kimura K., Hara H. ,and Watanabe Y. Removal of pharmaceutical compounds by submerged membrane bioreactors (MBRs). Desalination 178 (2005): 135-140.

Kimura K., Hara H. ,and Watanabe Y. Elimination of Selected Acidic Pharmaceuticals from Municipal Wastewater by an Activated Sludge System and Membrane Bioreactors. Environmental Science & Technology 41 (2007): 3708-3714.

Klavarioti M., Mantzavinos D. ,and Kassinos D. Removal of residual pharmaceuticals from aqueous systems by advanced oxidation processes. Environment International 35 (2009): 402-417.

Kosma C. I., Lambropoulou D.A. ,and Albanis T. A. Occurrence and removal of PPCPs in municipal and hospital wastewaters in Greece. Journal of Hazardous Materials 179 (2010): 804-817.

Laboratory Los Alamos National (2004). Magnetic Separation SPI: Waste Water Treatment.

Larson B.F. Magnetic material [Online] 2001-2010. Available from: http://www.ndt-ed.org/EducationResources/CommunityCollege/MagParticle/Physics/ MagneticMatls.htm,

Lee H.B., Peart T. E. ,and Svoboda M. L. Determination of endocrine-disrupting phenols, acidic pharmaceuticals, and personal-care products in sewage by solid-phase extraction and gas chromatography-mass spectrometry. <u>Journal of Chromatography A</u> 1094 (2005): 122-129.

Lin H.Y.,and Chen Y.W. Preparation of Spherical Hexagonal Mesoporous Silica. <u>Journal of Porous Materials</u> 12 (2005): 95-105.

Lindqvist N., Tuhkanen T. ,and Kronberg L. Occurrence of acidic pharmaceuticals in raw and treated sewages and in receiving waters. <u>Water Research</u> 39 (2005): 2219-2228.

Maria Chong A. S., Zhao X. S., Kustedjo A. T. ,and Qiao S. Z. Functionalization of large-pore mesoporous silicas with organosilanes by direct synthesis. <u>Microporous and Mesoporous Materials</u> 72 (2004): 33-42.

Martien D. (1994). Introduction to: AC Susceptibility, QuantumDesign.

Mascolo G., et al. Biodegradability of pharmaceutical industrial wastewater and formation of recalcitrant organic compounds during aerobic biological treatment. <u>Bioresource Technology</u> 101 (2010): 2585-2591.

Matamoros V., García J. ,and Bayona J. M. Organic micropollutant removal in a full-scale surface flow constructed wetland fed with secondary effluent. <u>Water Research</u> 42 (2008): 653-660.

Mitsuhashi K., Yoshizaki R., Okadab H., Oharac T. ,and Wada H. Purification Of Endocrine Disrupter-Polluted Water Using High Temperature Superconducting Hgms. <u>Physical Separation In Science And Engineering</u> 12 (2003): 205-213.

Moldovan Z. Occurrences of pharmaceutical and personal care products as micropollutants in rivers from Romania. <u>Chemosphere</u> 64 (2006): 1808-1817.

Mompelat S., Le Bot B. ,and Thomas O. Occurrence and fate of pharmaceutical products and by-products, from resource to drinking water. <u>Environment International</u> 35 (2009): 803-814.

Moorthy K. <u>Effect Of Surface Energy Of Fibers On Coalescence Filtration</u> Master of Science The Graduate Faculty of The University of Akron, The University of Akron, 2007.

Nakada N., et al. Removal of selected pharmaceuticals and personal care products (PPCPs) and endocrine-disrupting chemicals (EDCs) during sand filtration and ozonation at a municipal sewage treatment plant. <u>Water Research</u> 41 (2007): 4373-4382.

Nakada N., Tanishima T., Shinohara H., Kiri K. ,and Takada H. Pharmaceutical chemicals and endocrine disrupters in municipal wastewater in Tokyo and their removal during activated sludge treatment. Water Research 40 (2006): 3297-3303.

Özer A., Akkaya G. ,and Turabik M. Biosorption of Acid Blue 290 (AB 290) and Acid Blue 324 (AB 324) dyes on Spirogyra rhizopus. Journal of Hazardous Materials 135 (2006): 355-364.

Pinnavaia Peter T. Tanev ,and Thomas J. A Neutral Templating Route to Mesoporous Molecular Sieves Science 267 (1995): 865-867.

Punyapalakul P. ,and Satoshi T. Effect of organic grafting modification of haxagonal mesoporous silicate on haloacetic acid removal. Environment Engineering Research 41 (2004).

Punyapalakul P., Soonglerdsongpha S., Kanlayaprasit C., Ngamcharussrivichai C. ,and Khaodhiar S. Effects of crystalline structures and surface functional groups on the adsorption of haloacetic acids by inorganic materials. Journal of Hazardous Materials 171 (2009): 491-499.

Qu J., Liu G., Wang Y. ,and Hong R. Preparation of Fe3O4-chitosan nanoparticles used for hyperthermia. Advanced Powder Technology 21 (2010): 461-467.

Reclamation U.S. Department of the Interior Bureau of (2009). Secondary/Emerging Constituents Report, U.S. Department of the Interior Bureau of Reclamation.

Rivera-Jiménez S. M. ,and Hernández-Maldonado A. J. Nickel(II) grafted MCM-41: A novel sorbent for the removal of Naproxen from water. Microporous and Mesoporous Materials 116 (2008): 246-252.

Samuel D. F., and Osman M. A. Adsorption processes for water treatment Butterworth.1987

Santos J. L., Aparicio I. ,and Alonso E. Occurrence and risk assessment of pharmaceutically active compounds in wastewater treatment plants. A case study: Seville city (Spain). Environment International 33 (2007): 596-601.

Sevilla M., Alvarez S. ,and Fuertes A. B. Synthesis and characterisation of mesoporous carbons of large textural porosity and tunable pore size by templating mesostructured HMS silica materials. Microporous and Mesoporous Materials 74 (2004): 49-58.

Sim W. J., Lee J.W. ,and Oh J.E. Occurrence and fate of pharmaceuticals in wastewater treatment plants and rivers in Korea. Environmental Pollution 158 (2010): 1938-1947.

Stumpf M., Ternes T. A., Wilken R.D., Silvana V.R. ,and Baumann W. Polar drug residues in sewage and natural waters in the state of Rio de Janeiro, Brazil. The Science of The Total Environment 225 (1999): 135-141.

Tanev P. T. ,and Pinnavaia T. J. Mesoporous Silica Molecular Sieves Prepared by Ionic and Neutral Surfactant Templating: A Comparison of Physical Properties. Chemistry of Materials 8 (1996): 2068-2079.

Thommes S. L., Joan E. S., Martin A. T., and Matthias.T. Characterization of Porous Solids and Powders: Surface Area, Pore Size, and Density. Springer, 2004.

Tian H.,et al. Using shell-tunable mesoporous Fe3O4@HMS and magnetic separation to remove DDT from aqueous media. Journal of Hazardous Materials 171 (2009): 459-464.

Tixier C., Singer H. P., Oellers S., and Müller S. R. Occurrence and Fate of Carbamazepine, Clofibric Acid, Diclofenac, Ibuprofen, Ketoprofen, and Naproxen in Surface Waters. Environmental Science & Technology 37 (2003): 1061-1068.

Vogt C., Toprak M., Muhammed M., Laurent S., Bridot J. L. ,and Müller R. High quality and tuneable silica shell–magnetic core nanoparticles. Journal of Nanoparticle Research 12 (2010): 1137-1147.

Wootiwat L., Patiparn p.l and Pisut P.l. Study of coalescence process for treating lubricant oily wastewater by stainless steel fibrous coalescer. Department of Environmental Engineering, Chulalongkorn University, 2010.

Yu N. G., et al. One-pot synthesis of mesoporous organosilicas using sodium silicate as a substitute for tetraalkoxysilane. Microporous and Mesoporous Materials 72 (2004): 25-32.

Yu Z., Peldszus S. and Huck, Peter M. Adsorption characteristics of selected pharmaceuticals and an endocrine disrupting compound--Naproxen, carbamazepine and nonylphenol--on activated carbon. Water Research 42 (2008): 2873-2882.

Zou W., Bai H., Zhao L., Li K. ,and Han R. Characterization and properties of zeolite as adsorbent for removal of uranium(VI) from solution in fixed bed column. Journal of Radioanalytical and Nuclear Chemistry (2011): 1-10.

Appendices

Appendix A

Appendix A: Characteristic of Synthesized Adsorbents

<p align="center">**Table A-1** Raw data of BET isotherm of HMS-SP</p>

HMS-SP							
P/P_0	Vol. (cc/g)	P/P_0	Vol. (cc/g)	P/P_0	Vol. (cc/g)	P/P_0	Vol. (cc/g)
0.02807	124.218	0.52532	377.929	0.97524	681.114	0.47557	370.776
0.05063	139.099	0.55101	386.171	0.94978	648.729	0.45062	349.823
0.07902	156.349	0.57617	393.843	0.92584	610.625	0.42508	331.829
0.1007	166.136	0.59947	400.523	0.90053	576.308	0.3996	306.159
0.12559	176.393	0.62422	407.489	0.87431	548.485	0.37536	281.878
0.15113	186.418	0.64957	414.369	0.85089	527.739	0.35009	263.544
0.1741	195.173	0.67446	421.255	0.82498	508.108	0.3244	249.483
0.20052	205.191	0.69936	428.34	0.79979	492.061	0.30073	238.743
0.22596	214.931	0.7262	436.324	0.7743	478.446	0.27526	228.322
0.25031	224.405	0.75101	444.316	0.74738	466.568	0.24967	218.434
0.27619	234.597	0.77477	452.607	0.72448	457.8	0.22366	208.756
0.2997	244.481	0.80242	463.391	0.69859	449.222	0.2007	200.363
0.32684	257.438	0.82636	474.774	0.67566	442.507	0.1759	191.411
0.35076	270.566	0.84979	487.699	0.65018	435.745	0.15071	182.308
0.37455	287.717	0.87509	506.106	0.62512	429.277	0.12583	173.002
0.39987	311.071	0.90065	531.982	0.59984	423.086	0.09853	162.294
0.42445	332.75	0.92471	565.562	0.57494	416.754	0.07223	150.993
0.44921	348.051	0.94968	613.043	0.55047	410.183	0.04802	138.567
0.47695	360.358	0.97462	671.151	0.52341	402.185	0.02157	118.771
0.49968	369.071	0.99443	750.633	0.50002	393.424	-	-

Table A-2 Raw Data of BET Isotherm of A-HMS-SP

P/P_0	Vol. (cc/g)	P/P_0	Vol. (cc/g)	P/P_0	Vol. (cc/g)	P/P_0	Vol. (cc/g)
0.02653	41.2528	0.5265	123.776	0.97072	509.95	0.47589	121.884
0.0501	48.7535	0.55027	130.118	0.94962	491.61	0.45035	115.766
0.07591	54.4918	0.57553	137.309	0.92456	464.638	0.4247	110.36
0.10136	59.1204	0.59976	146.759	0.89866	444.176	0.39843	105.744
0.12654	63.1547	0.62512	156.219	0.87495	412.343	0.37339	101.359
0.15194	66.733	0.64965	166.692	0.8493	372.789	0.35029	98.4651
0.17701	70.2557	0.6763	180.589	0.82341	334.261	0.32303	94.4141
0.20194	73.4682	0.7025	193.927	0.79984	304.319	0.29779	90.7387
0.22689	76.5701	0.72749	207.569	0.77342	281.343	0.27247	87.3283
0.25183	79.6041	0.75164	224.069	0.74973	260.045	0.24755	83.7733
0.2766	82.561	0.77659	240.319	0.72563	241.844	0.22271	80.1585
0.302	85.4978	0.80113	258.61	0.69955	224.787	0.19698	76.8107
0.32623	89.0682	0.82436	278.751	0.67449	207.551	0.17264	73.2261
0.35169	92.2472	0.8499	302.66	0.65054	193.637	0.14747	69.4192
0.37692	95.5588	0.876	331.487	0.62414	176.95	0.12275	65.2689
0.40167	99.1129	0.8998	367.871	0.59809	162.175	0.09792	60.7274
0.42598	103.033	0.92542	410.94	0.57563	153.673	0.07311	55.6481
0.45024	107.035	0.9496	457.06	0.54865	142.749	0.04864	49.6538
0.47689	112.686	0.97479	502.421	0.52487	134.548	0.02478	41.4113
0.49964	117.635	0.99606	518.959	0.49966	128.242	-	-

Table A-3 Raw Data of BET Isotherm of M-HMS-SP

				M-HMS-SP			
P/P_0	Vol. (cc/g)	P/P_0	Vol. (cc/g)	P/P_0	Vol. (cc/g)	P/P_0	Vol. (cc/g)
0.02747	93.3261	0.52635	194.149	0.97406	406.342	0.47455	204.759
0.05166	109.721	0.55167	195.839	0.94938	342.147	0.44875	198.29
0.07524	121.122	0.57669	197.677	0.92418	298.649	0.42473	195.065
0.10035	131.34	0.60093	199.824	0.90029	276.382	0.39864	192.35
0.1257	140.128	0.62629	201.568	0.87075	264.076	0.37397	189.43
0.15161	147.671	0.65087	203.165	0.84873	256.54	0.34885	186.57
0.17643	153.923	0.67733	207.843	0.82379	249.724	0.32305	184.415
0.20157	159.784	0.70128	210.119	0.79758	244.399	0.2992	181.343
0.22733	164.209	0.72505	213.139	0.77564	240.426	0.27435	178.038
0.24952	168.223	0.75006	216.104	0.74977	236.437	0.24939	174.56
0.27542	171.285	0.7745	219.032	0.7251	232.873	0.2249	170.309
0.3008	173.903	0.79963	222.721	0.69706	231.434	0.20047	165.363
0.32499	177.2	0.82659	227.747	0.67317	229.034	0.17248	159.266
0.35105	179.749	0.85021	235.905	0.6492	226.406	0.14798	152.496
0.37624	181.74	0.87537	243.407	0.6242	223.537	0.12323	144.769
0.40172	183.546	0.90128	253.888	0.59898	220.805	0.09858	135.77
0.42647	185.329	0.92459	268.44	0.574	218.145	0.07424	125.424
0.45153	187.041	0.94995	300.276	0.54906	215.475	0.04995	112.662
0.47437	190.507	0.97469	371.54	0.52398	213.183	0.02375	93.0727
0.50111	192.327	0.99485	481.474	0.4964	212.05	-	-

Table A-4 Raw Data of BET Isotherm of P-HMS-SP

P-HMS-SP							
P/P_0	Vol. (cc/g)	P/P_0	Vol. (cc/g)	P/P_0	Vol. (cc/g)	P/P_0	Vol. (cc/g)
0.02561	92.4674	0.52525	209.124	0.97539	456.4674	0.47544	213.9723
0.04937	109.2765	0.55001	211.2985	0.95069	332.4804	0.44667	208.6786
0.07585	123.4021	0.57525	213.4176	0.92558	296.584	0.42466	205.814
0.09969	133.3932	0.6000	215.5563	0.89925	278.1542	0.39902	202.9152
0.12478	142.6036	0.62507	217.7194	0.87187	266.7015	0.37591	200.3344
0.14999	150.6835	0.65034	219.9388	0.84997	259.7586	0.3492	197.1534
0.17424	157.6337	0.67558	222.1558	0.82426	253.8401	0.32467	193.8271
0.19974	164.186	0.70026	224.3989	0.79526	248.6974	0.30057	190.2643
0.22522	170.1403	0.72709	228.4682	0.77572	245.5261	0.27365	185.562
0.25112	175.4535	0.75051	231.248	0.75074	241.9967	0.24868	180.7227
0.27525	180.8124	0.77441	234.4926	0.72514	238.7773	0.22456	175.3915
0.30225	185.4756	0.80215	238.6623	0.69295	235.4886	0.20023	169.5612
0.32501	188.8263	0.82646	242.9625	0.67483	233.6574	0.17552	163.0669
0.3507	192.2317	0.85168	247.5645	0.65048	231.2765	0.15024	155.4788
0.37432	194.9119	0.87444	255.5187	0.62558	228.9013	0.12517	147.2292
0.39935	197.4943	0.90088	265.5702	0.60007	226.6648	0.10022	137.9837
0.42496	199.8875	0.92505	279.7194	0.57486	224.5514	0.0759	127.4462
0.45077	202.0457	0.94956	306.0000	0.54456	222.1966	0.05017	113.9641
0.47581	204.0889	0.97495	376.2773	0.52371	220.4731	0.02523	95.8426
0.49925	206.9706	0.99554	614.7463	0.50017	218.4486	-	-

Table A-5 Raw Data of BET Isotherm of N-HMS-SP

				N-HMS-SP			
P/P_0	Vol. (cc/g)	P/P_0	Vol. (cc/g)	P/P_0	Vol. (cc/g)	P/P_0	Vol. (cc/g)
0.02637	74.5706	0.52631	207.9207	0.97454	580.2927	0.4759	211.1026
0.04958	89.8988	0.54929	211.8878	0.95069	434.647	0.45024	203.1217
0.07601	102.1287	0.57626	216.7921	0.92579	376.8783	0.42223	195.7784
0.10145	111.714	0.60094	221.5458	0.89971	347.3734	0.39847	190.4897
0.12714	120.4003	0.62573	226.3187	0.87457	325.9809	0.37564	185.8605
0.14961	127.0844	0.64988	231.3297	0.85062	311.3351	0.34978	181.1135
0.17417	134.0618	0.67504	240.3584	0.82253	298.7045	0.32548	176.0889
0.20107	142.1984	0.69906	246.041	0.80009	289.5663	0.30087	170.829
0.22476	148.223	0.72706	253.0438	0.77485	280.5923	0.27348	164.6512
0.24964	154.3037	0.752	259.5499	0.74807	272.2599	0.25088	159.3584
0.27492	159.9986	0.77653	266.7934	0.7219	264.8372	0.22456	152.8659
0.30053	165.5882	0.80085	274.4446	0.69879	259.7497	0.19952	146.3283
0.32584	170.8358	0.82416	283.197	0.67428	253.7962	0.17401	139.528
0.35128	175.8495	0.85055	294.8359	0.64912	247.9029	0.14979	132.4401
0.37617	180.7004	0.87493	307.4651	0.62387	242.2353	0.12546	124.7554
0.39931	184.9535	0.90046	325.104	0.59895	236.7155	0.10046	116.1709
0.42602	189.8919	0.92473	348.6676	0.57491	232.5595	0.07481	106.2539
0.44939	194.0602	0.9491	392.6895	0.54855	227.1163	0.04875	93.9384
0.4762	198.8947	0.97422	491.6156	0.52579	222.5007	0.02541	78.5516
0.49927	203.026	0.99468	745.0369	0.4985	216.9398	-	-

Table A-6 Raw Data of pHzpc of N-HMS-SP

pH	HMS-SP (mV)	A-HMS-SP (mV)	M-HMS-SP (mV)	P-HMS-SP (mV)	N-HMS-SP (mV)
3.02	13.76929	44.655	13.997	-	46.18579
3.95	5.80536	32.35945	11.87556	24.69364	8.58775
5.07	-8.12556	21.07455	10.04722	12.73233	-8.52714
6.11	-14.0983	16.33	7.55625	-7.60286	-13.1705
7.05	-16.69	11.94882	-13.63	-11.904	-14.5982
8	-22.6273	7.70775	-22.4375	-21.0111	-22.956
8.97	-24.7167	-9.86727	-23.13	-23.0625	-29.2357
9.99	-27.2444	-13.5448	-24.3111	-29.2091	-34.3286

Appendix B

Appendix B: Adsorption of NAX

Table B-1 Kinetic Data of HMS-SP

Time(min)	Conc.(mg/L)
0	2.66
30	2.62
60	2.53
120	2.50
180	2.49
240	2.49
360	2.50
540	2.48
720	2.49
1440	2.48

Table B-2 Kinetic Data of M-HMS-SP

Time(min.)	Conc.(mg/L)
0	3.22
1	2.59
3	2.52
5	2.40
10	2.38
15	2.36
20	2.33
60	2.24
180	2.34
540	2.29
720	2.27
1200	2.26
1440	2.28

Table B-3 Kinetic Data of A-HMS-SP

Time(min.)	Conc.(mg/L)
0	4.52
2	4.51
4	4.51
7	4.49
10	4.49
20	4.49
30	4.50
45	4.48

Table B-3(Continued) Kinetic Data of A-HMS-SP

Time(min.)	Conc.(mg/L)
60	4.48
180	4.46
540	4.46
1410	4.46

Table B-4 Kinetic Data of P-HMS-SP

Time(min.)	Conc.(mg/L)
0	3.11
1	3.02
3	2.78
5	2.62
10	2.42
20	2.16
30	1.94
60	1.37
180	1.21
540	1.15
1140	1.11
1440	1.11

Table B-5 Kinetic Data of N-HMS-SP

Time(min.)	Conc.(mg/L)
0	3.02
1	3.00
3	2.96
5	2.96
10	2.96
15	2.95
30	2.94
60	2.95
120	2.94
180	2.95
360	2.94
540	2.93
720	2.92
1440	2.95

Table B-6 Kinetic Data of PAC

Time(min.)	Conc.(mg/L)
0	9.84
1	6.75
2	6.40
3	5.81
5	5.63
10	4.95
15	4.63
25	4.07
60	2.94
360	1.54
420	1.03
540	0.93
540	1.02
720	0.85
840	0.84
1440	0.83

Table B-7 Isotherm Data of HMS-SP

pH5		pH7		pH9	
Eq.Conc.(mg/L)	q (mg/g)	Eq.Conc.(mg/L)	q (mg/g)	Eq.Conc.(mg/L)	q (mg/g)
0.49	0	0.59	0.006	0.65	0
0.88	0.087	0.91	0.050	0.96	0
2.50	0.201	2.66	0.123	1.18	0
7.53	0.398	2.91	0.134	3.22	0
5.96	0.343	4.48	0.149	4.69	0
8.67	0.433	8.28	0.241	7.70	0
-	-	9.41	0.284	8.91	0

Table B-8 Isotherm Data of M-HMS-SP

pH5		pH7		pH9	
Eq.Conc.(mg/L)	q (mg/g)	Eq.Conc.(mg/L)	q (mg/g)	Eq.Conc.(mg/L)	q (mg/g)
0.33	0.214	0.25	0.014	0.50	0.000
0.43	0.196	0.60	0.073	0.62	0.068
0.59	0.358	0.73	0.131	2.75	0.178
1.58	1.127	2.50	0.466	4.54	0.230
2.70	1.435	2.51	0.476	7.45	0.533
4.17	2.545	3.41	0.560	-	-
5.15	2.748	6.48	1.281	-	-
-	-	7.08	1.377	-	-

Table B-9 Isotherm Data of A-HMS-SP

pH5		pH7		pH9	
Eq.Conc.(mg/L)	q (mg/g)	Eq.Conc.(mg/L)	q (mg/g)	Eq.Conc.(mg/L)	q (mg/g)
0.64	0	0.58	0	0.72	0
0.97	0.014	0.62	0	5.09	0
1.90	0.029	0.60	0	10.13	0
2.98	0.045	0.89	0.003	-	-
6.01	0.116	2.78	0.015	-	-
8.49	0.131	4.03	0.021	-	-
9.81	0.151	8.72	0.043	-	-

Table B-10 Isotherm Data of P-HMS-SP

pH5		pH7		pH9	
Eq.Conc.(mg/L)	q (mg/g)	Eq.Conc.(mg/L)	q (mg/g)	Eq.Conc.(mg/L)	q (mg/g)
0.24	0.271	0.15	0.179	0.68	0
0.31	1.318	0.42	0.486	0.89	0
0.53	3.024	5.92	3.166	1.06	0
0.68	3.722	1.36	1.288	2.72	0.223
1.14	4.915	2.26	1.856	3.95	0.600
1.38	5.510	4.61	2.491	6.74	1.170
2.26	6.740	-	-	7.83	1.618
2.79	7.357	-	-	-	-

Table B-11 Isotherm Data of N-HMS-SP

pH5		pH7		pH9	
Eq.Conc.(mg/L)	q (mg/g)	Eq.Conc.(mg/L)	q (mg/g)	Eq.Conc.(mg/L)	q (mg/g)
0.66	0	0.67	0	0.72	0
2.02	0.225	4.91	0.084	2.83	0.050
5.65	0.565	9.23	0.227	5.62	0.096
7.22	0.802	9.63	0.261	8.11	0.156
8.67	1.010	11.66	0.614	9.87	0.166

Table B-12 Isotherm Data of PAC

pH5		pH7		pH9	
Eq.Conc.(mg/L)	q (mg/g)	Eq.Conc.(mg/L)	q (mg/g)	Eq.Conc.(mg/L)	q (mg/g)
0	6.550	0.00	8.567	0	6.852
0	14.895	0.02	13.988	0.00	17.346
0	45.429	0.02	50.615	0.02	53.961
0	68.554	0.03	68.218	0.14	90.309
0	144.566	0.18	116.342	0.38	103.562
0.33	170.831	0.15	117.827	1.15	164.934

Table B-12 Intraparticle Diffusion Data of HMS-SP, M-HMS-SP and A-HMS-SP

HMS-SP		M-HMS-SP		A-HMS-SP	
$t^{1/2}$ $(min)^{1/2}$	q (mg/g)	$t^{1/2}$ $(min)^{1/2}$	q (mg/g)	$t^{1/2}$ $(min)^{1/2}$	q (mg/g)
5.48	0.02	1.00	0.47	1.41	0.00
7.75	0.09	1.73	0.52	2.00	0.01
10.95	0.11	2.24	0.62	4.47	0.02
13.42	0.13	3.16	0.63	6.71	0.03
15.49	0.12	3.87	0.64	7.75	0.03
18.97	0.12	4.47	0.66	13.42	0.04
23.24	0.13	26.83	0.71	23.24	0.04
26.83	0.13	34.64	0.72	37.55	0.04
37.95	0.13	-	-	-	-

Table B-13 Intraparticle Diffusion Data of P-HMS-SP, N-HMS-SP and PAC

P-HMS-SP		N-HMS-SP		PAC	
$t^{1/2}$ $(min)^{1/2}$	q (mg/g)	$t^{1/2}$ $(min)^{1/2}$	q (mg/g)	$t^{1/2}$ $(min)^{1/2}$	q (mg/g)
1.00	0.07	1.00	0.06	1.00	46.32
1.73	0.25	1.73	0.08	1.41	51.58
2.24	0.37	2.24	0.11	1.73	60.49
3.16	0.52	3.16	0.11	2.24	63.10
4.47	0.72	3.87	0.11	3.16	73.27
5.48	0.88	5.48	0.12	3.87	78.18
7.75	1.31	10.95	0.12	5.00	86.48
13.42	1.43	18.97	0.12	7.75	103.43
23.24	1.48	23.24	0.13	18.97	124.51
33.76	1.50	26.83	0.13	20.49	132.20

Table B-13(Continued) Intraparticle Diffusion Data of P-HMS-SP, N-HMS-SP and PAC

P-HMS-SP		N-HMS-SP		PAC	
$t^{1/2}$ $(min)^{1/2}$	q (mg/g)	$t^{1/2}$ $(min)^{1/2}$	q (mg/g)	$t^{1/2}$ $(min)^{1/2}$	q (mg/g)
37.95	1.51	37.95	0.14	23.24	133.68
-	-	-	-	23.24	132.33
-	-	-	-	26.83	134.81
-	-	-	-	28.98	134.94
-	-	-	-	37.95	135.11

Table B-14 Standard Curve Data of NAX

pH5		pH7		pH9	
Conc.(mg/L)	Abs.	Conc.(mg/L)	Abs.	Conc.(mg/L)	Abs.
0.5	0.145	0.5	0.122	0.5	0.127
1	0.304	1	0.292	1	0.262
5	1.56	5	1.552	5	1.504
10	3.284	10	3.248	10	3.264

Figure B-1 Standard Curve of NAX at pH 5
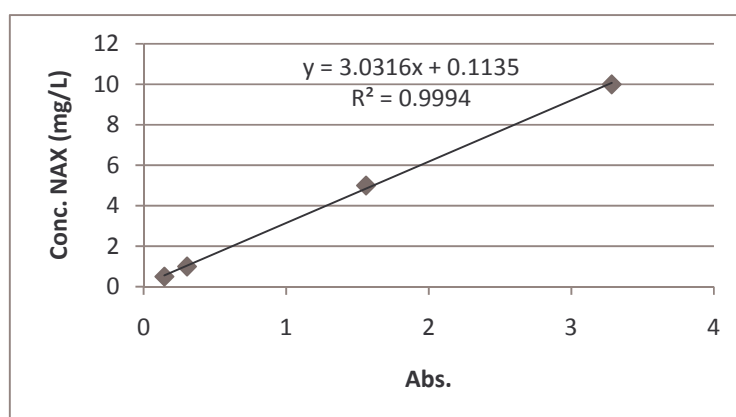
Figure B-2 Standard Curve of NAX at pH 7
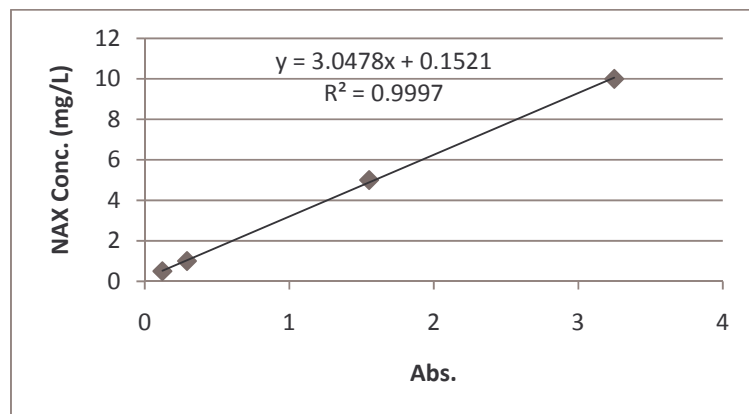
Figure B-3 Standard Curve of NAX at pH 9
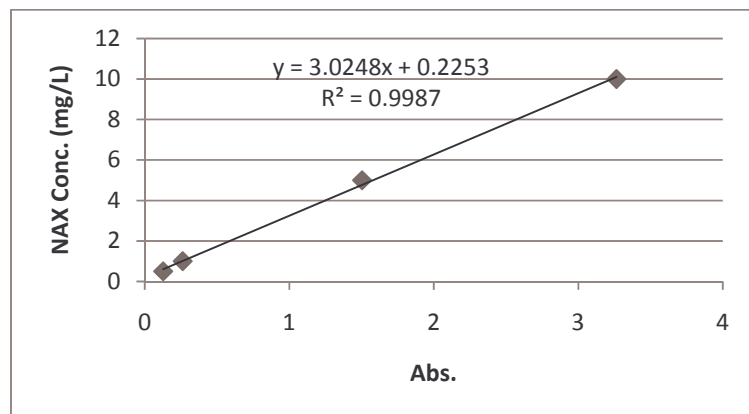
Appendix C

Appendix C: Adsorption of NAX

Table C-1 Breakthrough Data of Variation Depth Filter at 0.5g/L of Particle
Concentration, 37.23 Cm^2 of Surface Area of Filter and 0.95cm/min of Flow Rate

5cm		3cm		1.5cm	
Vol.(mL)	C/C$_0$	Vol.(mL)	C/C$_0$	Vol.(mL)	C/C$_0$
29	0.00	29	0.02	29	0.00
58	0.00	58	0.01	58	0.00
86	0.01	86	0.02	86	0.00
115	0.01	115	0.01	115	0.08
144	0.05	144	0.03	144	0.16
173	0.06	173	0.05	173	0.28
202	0.06	202	0.10	202	0.38
230	0.09	230	0.18	230	0.47
259	0.11	259	0.26	259	0.58
288	0.21	288	0.42	288	0.61
317	0.28	317	0.47	317	0.65
346	0.40	346	0.59	346	0.73
374	0.44	374	0.67	374	0.86
403	0.56	403	0.77	403	0.95
432	0.59	432	0.81	432	0.95
461	0.62	461	0.86	461	0.97
490	0.71	490	0.90	490	1.01
518	0.77	518	1.00	518	1.06
547	0.79	547	1.01	-	-
576	0.84	-	-	-	-
605	1.00	-	-	-	-
634	1.01	-	-	-	-
662	1.02	-	-	-	-

Table C-2 Breakthrough Data of Variation Flow Rate at 0.5g/L of Particle Concentration, 37.23 cm^2 of Surface Area of Filter and 5 cm of Depth Filter

0.75 cm/min		0.95 cm/min		1.25 cm/min	
Time(min.)	C/C$_0$	Time(min.)	C/C$_0$	Time(min.)	C/C$_0$
1	0.02	1	0.00	1	0.04
2	0.03	2	0.00	2	0.04
3	0.02	3	0.01	3	0.06
4	0.02	4	0.01	4	0.08
5	0.02	5	0.05	5	0.13
6	0.02	6	0.06	6	0.19
7	0.05	7	0.06	7	0.31
8	0.05	8	0.09	8	0.39
9	0.07	9	0.11	9	0.56
10	0.09	10	0.21	10	0.66
11	0.10	11	0.28	11	0.71
12	0.11	12	0.40	12	0.77
13	0.13	13	0.44	13	0.80
14	0.18	14	0.56	14	0.93
15	0.19	15	0.59	15	0.98
16	0.21	16	0.62	16	1.04
17	0.21	17	0.71	17	1.06
18	0.21	18	0.77	18	-
19	0.22	19	0.79	19	-
21	0.24	21	0.84	21	-
22	0.24	22	1.00	22	-
24	0.26	24	1.01	24	-
25	0.28	25	1.02	25	-

Table C-2 (Continued) Breakthrough Data of Variation Flow Rate at 0.5g/L of Particle Concentration, 37.23 cm^2 of Surface Area of Filter and 5 cm of Depth Filter

0.75 cm/min		0.95 cm/min		1.25 cm/min	
Time(min.)	C/C$_0$	Time(min.)	Time(min.)	C/C$_0$	Time(min.)
26	0.34	26	-	26	-
27	0.39	27	-	27	-
28	0.38	28	-	28	-
29	0.39	29	-	29	-
30	0.44	30	-	30	-
32	0.44	32	-	32	-
33	0.48	33	-	33	-
34	0.50	34	-	34	-
35	0.51	35	-	35	-
36	0.51	36	-	36	-
37	0.52	37	-	37	-
38	0.54	38	-	38	-
39	0.55	39	-	39	-
40	0.60	40	-	40	-
41	0.59	41	-	41	-
42	0.63	42	-	42	-
43	0.64	43	-	43	-
44	0.67	44	-	44	-
45	0.70	45	-	45	-
46	0.70	46	-	46	-
48	0.71	48	-	48	-
50	0.72	50	-	50	-
51	0.78	51	-	51	-

Table C-2 (Continued) Breakthrough Data of Variation Flow Rate at 0.5g/L of Particle Concentration, 37.23 cm^2 of Surface Area of Filter and 5 cm of Depth Filter

0.75 cm/min		0.95 cm/min		1.25 cm/min	
Time(min.)	C/C$_0$	Time(min.)	C/C$_0$	Time(min.)	C/C$_0$
52	0.82	52	-	52	-
53	0.84	53	-	53	-
54	0.90	54	-	54	-
55	0.94	55	-	55	-
56	0.99	56	-	56	-
57	1.05	57	-	57	-
58	1.08	58	-	58	-

Table C-3 Breakthrough Data of Variation Surface Area of Filter at 0.5g/L of Particle Concentration, 0.95cm/min of Flow Rate and 5 cm of Depth Filter

49.66 cm^2		37.23 cm^2		19.32 cm^2	
Vol.(mL)	C/C$_0$	Vol.(mL)	C/C$_0$	Vol.(mL)	C/C$_0$
29	0.11	29	0.00	29	0.03
58	0.12	58	0.00	58	0.06
86	0.12	86	0.01	86	0.06
115	0.13	115	0.01	115	0.05
144	0.16	144	0.05	144	0.05
173	0.17	173	0.06	173	0.06
202	0.20	202	0.06	202	0.07
230	0.23	230	0.09	230	0.07
259	0.24	259	0.11	259	0.10
288	0.29	288	0.21	288	0.17
317	0.35	317	0.28	317	0.26
346	0.42	346	0.40	346	0.36
374	0.46	374	0.44	374	0.39

Table C-3 (Continued) Breakthrough Data of Variation Surface Area of Filter at 0.5g/L of Particle Concentration, 0.95cm/min of Flow Rate and 5 cm of Depth Filter

49.66 cm^2		37.23 cm^2		19.32 cm^2	
Vol.(mL)	C/C$_0$	Vol.(mL)	Vol.(mL)	C/C$_0$	Vol.(mL)
403	0.55	403	0.56	403	0.51
432	0.61	432	0.59	432	0.60
461	0.64	461	0.62	461	0.62
490	0.69	490	0.71	490	0.65
518	0.70	518	0.77	518	0.70
547	0.75	547	0.79	547	0.75
576	0.78	576	0.84	576	0.80
605	0.87	605	1.00	605	0.88
634	0.93	634	1.01	634	0.91
662	0.96	662	1.02	662	0.93
691	0.97	-	-	-	-

Table C-4 Breakthrough Data of Variation Particle Concentration at 0.95cm/min of Flow Rate, 37.23 cm^2 of Surface Area of Filter and 5 cm of Depth Filter

0.3g/L		0.5 g/L		1 g/L	
Vol.(mL)	C/C$_0$	Vol.(mL)	C/C$_0$	Vol(ml.)	C/C$_0$
29	0.01	29	0.00	29	0.02
58	0.01	58	0.00	58	0.01
86	0.01	86	0.01	86	0.02
115	0.02	115	0.01	115	0.02
144	0.03	144	0.05	144	0.05
173	0.03	173	0.06	173	0.09
202	0.03	202	0.06	202	0.12
230	0.03	230	0.09	230	0.25

Table C-4 (Continued) Breakthrough Data of Variation Particle Concentration at 0.95cm/min of Flow Rate, 37.23 cm^2 of Surface Area of Filter and 5 cm of Depth Filter

0.3g/L		0.5 g/L		1 g/L	
Vol.(mL)	C/C$_0$	Vol.(mL)	Vol.(mL)	C/C$_0$	Vol.(mL)
259	0.04	259	0.11	259	0.40
288	0.04	288	0.21	288	0.49
317	0.05	317	0.28	317	0.59
346	0.06	346	0.40	346	0.68
374	0.07	374	0.44	374	0.73
403	0.03	403	0.56	403	0.86
432	0.05	432	0.59	432	1.00
461	0.05	461	0.62	461	1.02
490	0.07	490	0.71	490	1.04
518	0.10	518	0.77	-	-
547	0.11	547	0.79	-	-
576	0.14	576	0.84	-	-
605	0.15	605	1.00	-	-
634	0.18	634	1.01	-	-
662	0.25	662	1.02	-	-
691	0.33	-	-	-	-
720	0.36	-	-	-	-
749	0.39	-	-	-	-
778	0.41	-	-	-	-
806	0.44	-	-	-	-
835	0.49	-	-	-	-
864	0.50	-	-	-	-
893	0.54	-	-	-	-

Table C-4 (Continued) Breakthrough Data of Variation Particle Concentration at 0.95cm/min of Flow Rate, 37.23 cm^2 of Surface Area of Filter and 5 cm of Depth Filter

0.3g/L		0.5 g/L		1 g/L	
Vol.(mL)	C/C$_0$	Vol.(mL)	C/C$_0$	Vol.(mL)	C/C$_0$
922	0.58	-	-	-	-
950	0.65	-	-	-	-
979	0.71	-	-	-	-
1008	0.73	-	-	-	-
1037	0.76	-	-	-	-
1123	0.84	-	-	-	-
1152	0.86	-	-	-	-
1210	0.92	-	-	-	-
1238	0.94	-	-	-	-
1267	0.94	-	-	-	-
1296	0.95	-	-	-	-
1325	0.97	-	-	-	-
1354	0.98	-	-	-	-

Table C-5 Breakthrough Data of without NAX and with NAX Particle Concentration at 0.95cm/min of Flow Rate, 37.23 cm^2 of Surface Area of Filter and 5 cm of Depth Filter

NAX		Non NAX	
Vol.(mL)	C/C$_0$	Vol.(mL)	C/C$_0$
29	0.00	29	0.00
58	0.00	58	0.00
86	0.02	86	0.00
115	0.04	115	0.08

Table C-5 (Continued) Breakthrough Data of without NAX and with NAX Particle Concentration at 0.95cm/min of Flow Rate, 37.23 cm^2 of Surface Area of Filter and 5 cm of Depth Filter

NAX		Non NAX	
Vol.(mL)	C/C$_0$	Vol.(mL)	C/C$_0$
144	0.11	144	0.16
173	0.19	173	0.28
202	0.24	202	0.38
230	0.27	230	0.47
259	0.34	259	0.58
288	0.43	288	0.61
317	0.49	317	0.65
346	0.62	346	0.73
374	0.65	374	0.86
403	0.71	403	0.95
432	0.74	432	0.95
461	0.78	461	0.97
490	0.88	490	1.01
518	0.93	518	1.06
547	0.94	-	-

BIOGRAPHY

Name: Ms. Waritta Ruangtrakul

Date of Birth: November 18, 1987

Nationality: Thai

University Education: 2005-2009 Bachelor's Degree, Department of Environmental Engineering, Faculty of Engineering Chulalongkorn University, Bangkok, Thailand

Presentation: Waritta Ruangtrakul and Patiparn Punyapalakul. *Adsorption Of Naproxen By Superparamagnetic Mesoporous Silicates.* The 10th National Environmental Conference (NEC10), 2011, Songkha, Thailand, March 23-25. Organized by The Environmental Engineering Association of Thailand.